Mechanisms of Ageing and Development 160 (2016) 93–116

Contents lists available at ScienceDirect

Mechanisms of Ageing and Development

journal homepage: www.elsevier.com/locate/mechagedev

Review

Longitudinal imaging of the ageing mouse

E. Dall'Ara[a,b,*], M. Boudiffa[a], C. Taylor[c], D. Schug[d], E. Fiegle[d], A.J. Kennerley[e], C. Damianou[f], G.M. Tozer[a], F. Kiessling[d], R. Müller[c]

[a] Department of Oncology and Metabolism, University of Sheffield, Sheffield, UK
[b] INSIGNEO Institute for in silico Medicine, University of Sheffield, Sheffield, UK
[c] Institute for Biomechanics, ETH Zurich, Zurich, Switzerland
[d] Institute for Experimental Molecular Imaging, RWTH Aachen University, Aachen, Germany
[e] Biological Services Unit, University of Sheffield, Sheffield, UK
[f] Department of Electrical Engineering, Cyprus University of Technology, Limassol, Cyprus

ARTICLE INFO

Article history:
Received 5 February 2016
Received in revised form 30 July 2016
Accepted 4 August 2016
Available online 13 August 2016

Keywords:
In vivo
Imaging
Mouse
Ageing
Longitudinal

ABSTRACT

Several non-invasive imaging techniques are used to investigate the effect of pathologies and treatments over time in mouse models. Each preclinical *in vivo* technique provides longitudinal and quantitative measurements of changes in tissues and organs, which are fundamental for the evaluation of alterations in phenotype due to pathologies, interventions and treatments. However, it is still unclear how these imaging modalities can be used to study ageing with mice models. Almost all age related pathologies in mice such as osteoporosis, arthritis, diabetes, cancer, thrombi, dementia, to name a few, can be imaged *in vivo* by at least one longitudinal imaging modality. These measurements are the basis for quantification of treatment effects in the development phase of a novel treatment prior to its clinical testing. Furthermore, the non-invasive nature of such investigations allows the assessment of different tissue and organ phenotypes in the same animal and over time, providing the opportunity to study the dysfunction of multiple tissues associated with the ageing process.

This review paper aims to provide an overview of the applications of the most commonly used *in vivo* imaging modalities used in mouse studies: micro-computed-tomography, preclinical magnetic-resonance-imaging, preclinical positron-emission-tomography, preclinical single photon emission computed tomography, ultrasound, intravital microscopy, and whole body optical imaging.

Contents

* Corresponding author at: Department of Oncology and Metabolism, University of Sheffield, Sheffield, UK.
E-mail addresses: e.dallara@sheffield.ac.uk (E. Dall'Ara), m.boudiffa@sheffield.ac.uk (M. Boudiffa), carly.taylor@hest.ethz.ch (C. Taylor), dschug@ukaachen.de (D. Schug), efiegle@ukaachen.de (E. Fiegle), a.j.kennerley@sheffield.ac.uk (A.J. Kennerley), christakis.damianou@cut.ac.cy (C. Damianou), g.tozer@sheffield.ac.uk (G.M. Tozer), fkiessling@ukaachen.de (F. Kiessling), ram@ethz.ch (R. Müller).

http://dx.doi.org/10.1016/j.mad.2016.08.001

1. Purpose of the review

1.1. Ageing mice and their application in preclinical research

Animal models, in particular mouse models, of human disease have become a fundamental component of preclinical research. Mice have a similar anatomy and physiology to humans when compared to other non-mammalian models such as drosophila and zebrafish (Rosenthal and Brown, 2007). However, most importantly, many biological processes and pathways are conserved between mice and humans including those most related to metabolism and stress response, two of the overriding aspects of disease progression. Additionally, mice and humans share over 95% of their genes, which paired with decades of genetic studies make mice a formidable tool for the investigation of mammalian gene function in health and disease (Justice et al., 2011; Rosenthal and Brown, 2007). Murine models can allow researchers to investigate the effect of pathologies and treatments in a more detailed manner than it is possible in clinical studies. Changes in tissues and can be tracked organs over time, with high accuracy and non-invasively. For a large body of human diseases, the primary or major risk factor implicated in disease development is ageing (Niccoli and Partridge, 2012). Age related diseases pose a huge socio-economic burden for both developed and developing nations. For example, in the UK in 2013, the overall economic impact of dementia was 26.3 billion pounds and with analysts forecasting continued increases in ageing populations, the burden posed by these diseases is only expected to rise (Prince et al., 2014; Suman and Beard, 2011). Therefore, it is sensible for researchers to move towards the use of aged mice in order to better understand age related diseases. The term "age related disease" covers an extremely broad field of study and to complement this, a broad range of novel aged mouse models will be required. Aged mice themselves are a relatively novel concept and their use will yield a whole host of new challenges with regards to their development, care and phenotyping. Additionally, the high costs associated with the time required to develop genetically modified models makes the choice of the appropriate model fundamentally important (Benjamin et al., 2006). Extensive systems are already in place for the study of a huge number of phenotypes in mice (Ayadi et al., 2012; Ferruzzi et al., 2013; Hoit, 2004; Lee et al., 2014; Raman et al., 2007; Rozman et al., 2014; Schofield et al., 2012), but to move forwards and tackle new challenges, scientists rely on the continual development of novel technique that can help them study and understand mice in increasingly robust and efficient ways. One group of techniques that is playing an increasingly important role in facilitating the use of aged mice models is that based around *in vivo* imaging. Indeed, there is a growing interest in applying *in vivo* imaging modalities to study ageing in laboratory mice, in order to acquire a more comprehensive understanding of the mechanisms involved in the ageing process and identify dysfunction of multiple tissues (Lin et al., 2014), to identify biomarkers of early onset of age related diseases (Lai et al., 2004)

and to test novel interventions (Stodieck et al., 2014; Zhang et al., 2015). These techniques can be used for providing both anatomical and functional information from the cellular level up to the whole organism. Thanks to the improvement over the past years, some of these modalities (*e.g.* functional or molecular imaging) have largely increased their time and space resolution, being close now to physical limits of dose or field strengths. *In vivo* imaging can be applied to study different aspects of ageing and the approaches presented in this review can be combined in order to quantitatively characterize the tissues and organ phenotypes longitudinally, leading to a comprehensive investigation of age-related dysfunction of multiple tissues. In addition, these methods applied to mice models have the potential of evaluating healthy ageing and frailty, which are difficult to assess in humans, providing a framework to test the effect of novel interventions on several end points.

2. *In vivo* imaging techniques

2.1. Methods

This review focuses on the most commonly used *in vivo* imaging techniques that can be applied pre-clinically to mouse models and can be used for the study of ageing: micro computed tomography (micro-CT), preclinical magnetic resonance imaging (preclinical-MRI), preclinical positron emission tomography (preclinical-PET), preclinical Single Photon Emission Computed Tomography (SPECT), ultrasound (US), intravital microscopy and whole body optical fluorescence imaging. As the topic is very broad and specific reviews can be found with details about each technique, the goal of this manuscript is to provide an overview of the available imaging modalities, without going into the details of the physics behind each technique. In addition, we will highlight the potential for combining modalities and investigating the same animal longitudinally in order, for example, to study dysfunction of multiple tissues associated with ageing. In the following seven sections, the review aims to underline the breadth of applications for the most used *in vivo* imaging techniques, their main applications, potential and limitations.

In Section 3 and Table 1 we report the advantages and limitations of the application of such techniques to study ageing or age-related pathologies in mouse models.

2.2. Preclinical micro computed tomography (micro-CT)

2.2.1. Technique

Micro-computed tomography (micro-CT) is an X-ray imaging modality that allows the non-destructive analysis of the 3D architectural properties of an object. The sample or animal to be scanned is placed between a microfocus X-ray tube, which emits X-rays collimated and filtered to narrow the energy spectrum, and a 2D charge-coupled device (CCD) array, which records the attenuated X-Rays after passing through the scanned object. The object is rotated during the scan and the projections taken in each scanning position are reconstructed into a 3D image. In the last two decades, and with an achievable isotropic voxel size down to about one micron, micro-CT has become the gold standard approach for evaluating 3D micro-architectural properties of small animal bones (Bouxsein et al., 2010). This imaging modality is routinely used *ex-vivo*, in endpoint animal studies of bone diseases, to primarily assess the effect of interventions on bone health (Pierroz et al., 2010; Sugiyama et al., 2008). More recently, the use of *in-vivo* micro-CT has proven extremely valuable in monitoring, non-invasively, spatio-temporal changes in bone micro-structure with age and/or disease (Fig. 1-A,B). It has the advantage that, by measuring the properties of the same bone, of the same animal, over time, the quantities can be normalized with respect to the baseline values (Fig. 1-D), correcting for the intrinsic initial variability of the animals assigned to different groups (Glatt et al., 2007; Silva et al., 2012).

With voxel sizes down to 9 μm, this technique can measure efficiently the size and distribution of small bone features such as trabeculae. Moreover, once applied to the mouse, the whole vertebrae (Lambers et al., 2012; Schulte et al., 2011) and long bones (Lu et al., 2015a) can be scanned, guaranteeing more comprehensive analyses in those specific anatomical sites.

2.2.2. Applications for mineralized tissues

In vivo micro-CT has been already used in mice to study the effect on the bone microarchitecture and density of musculoskeletal pathologies related to ageing such as osteoporosis (Klinck and Boyd, 2008), fractures (He et al., 2011) and bone metastases (Ravoori et al., 2010). Furthermore, this technique has been used for studying the effect of pharmacological treatments (Stadelmann et al., 2011) and of external loading (Silva et al., 2012; Willie et al., 2013) on calcified (hard) tissues. In particular, Klinck and Boyd (2008) used *in vivo* micro-CT scans of the proximal tibia for assessing the magnitude of bone changes due to ovariectomy in different inbred mice strains, in order to select the best mouse model of accelerated bone loss. In two other studies, Silva et al. (2012) and Willie et al. (2013) investigated the effect of *in vivo* mechanical loading of the mouse tibia on the related longitudinal bone changes in the trabecular and cortical compartments, in function of ageing. Similarly, Stadelmann et al. (2011) studied the effect of combined *in vivo* loading and injections of zoledronate on the properties of the cortical bone of the mouse tibia. Furthermore, He et al. (2011) have used *in vivo* micro-CT to investigate bone healing in a defect-induced mouse femur model, showing the defect-closing rate on the same animals tracked over time. Ravoori et al. (2010) showed how induced prostate cancer affects the bone mineral density in a mouse model by using low resolution *in vivo* micro-CT. Moreover, if coupled with advanced image processing techniques, such as image registration, *in-vivo* micro-CT imaging can improve the precision of bone parameter measurements, therefore increasing the sensitivity to detect changes in the bone micro-architecture following intervention (Baiker et al., 2011; Campbell et al., 2014). This technique can also provide low resolution scans of the whole skeleton (Fig. 1-C1) and high resolution scans of the whole bones *in vivo* (Fig. 1-C2,C3,C4), and allows users to generate subject specific computational models for non-invasive estimation of bone strength as well as local mechanical properties associated with ageing (Lambers et al., 2012, 2015; Razi et al., 2015) or different interventions (Levchuk et al., 2014; Willie et al., 2013; Yang et al., 2014).

2.2.3. Applications for soft tissues

Although bone imaging is the most common *in vivo* micro-CT application, increasing evidence shows that non-mineralized (soft) tissues can also be imaged, provided there is sufficient contrast between the tissue of interest and the surrounding areas (Bouxsein et al., 2010). These methods allow micro-CT to be used for the study of some soft tissues related to pathologies such as, for example, osteoarthritis, atherosclerosis and lung tumours. Many soft tissues have been scanned *ex vivo* with or without contrast agents: soft tissue of the paw (Perilli et al., 2015), angiogenesis (Gayetskyy et al., 2014) and cartilage (Marenzana et al., 2014) are examples. However, only a few of these procedures are applicable *in vivo*. One approach is to use the intrinsic heterogeneity of the native contrast that some tissues possess, as for lung imaging or adipose tissue. For example, the lung tissue has the particularity of presenting a good contrast with the air it is filled with. *In vivo* lung imaging, combined with custom image processing algorithms, provides a good tool to study lung function in acute and chronic small animal pul-

Table 1
Summary of the specifications, main advantages and main limitations of the preclinical *in vivo* imaging techniques presented in this review, with particular emphasis on the applications for studying ageing or age-related diseases with mouse models.

Preclinical *In vivo* imaging modality	Imaging Time	Maximal resolution	Advantages	Disadvantages	Main Longitudinal applications associated to ageing and age-related diseases	Examples
Micro CT	min-h	~0.01 mm (organ) ~0.1 mm (body)	Very good spatial resolution Good sensitivity	Long scanning time Potential moving artifacts Radiation exposure Limited number of contrast agents for *in vivo* applications	Osteoporosis and remodeling Bone metastasis Neurodegenerative diseases Lung and liver tumour progression Bone regeneration (combined with SPECT)	Klinck and Boyd (2008); Silva et al., (2012); Willie et al. (2013) Ravoori et al. (2010) Starosolski et al. (2015) Lalwani et al. (2013) Ohta et al. (2006) He et al. (2011); Lienemann et al. (2015)
Micro MRI	min-h	~0.1 mm (in plane)	Good spatial resolution Contrast agents can be used	Long scanning time Potential moving artifacts Poor sensitivity (can be improved with contrast agents)	Alzheimer's disease Cardiac structure and function Decreased brain function	Maheswaran et al. (2009) Schneider et al. (2008) Sorond et al. (2011)
PET	min	~1 mm	High sensitivity Many radiotracers	Poor spatial resolution Requires specialized radiochemistry Radiation exposure	Alzheimer's disease Parkinson's disease Atherosclerosis Type 2 diabetes	Fodero-Tavoletti et al. (2011) Waerzeggers et al. (2010) Wenning et al. (2014) Yong et al. (2011)
SPECT	min	~1 mm	Good sensitivity (lower than PET)	Fewer radiochemicals compared to PET Radiation exposure	Parkinson's disease Alzheimer's disease Oncology Bone regeneration (combined with microCT)	Hwang et al. (2002) Shimizu et al. (2016) Bernsen et al. (2014) Lienemann et al. (2015)
Ultrasound	s	0.5 mm (3 MHz) 0.15 mm (10 MHz)	Great temporal resolution. Portable no long-term side effects Relatively cheap	Poor depth-of-field for high resolution imaging (high frequency). Poor bone and air penetration. The method is operator-dependent	Liver diseases Cardiac fibrosis Hydronephrosis	Fernandez-Dominguez et al. (2011) Johnson et al. (2013) Springer et al. (2014)
Optical intravital microscopy	s	<0.01 mm	Real time imaging Very high resolution Good sensitivity Many contrast agents Relatively cheap	2D technique requires surgery	Cortical plasticity Beating heart Atherosclerosis and myocardial infarction	Stodieck et al. (2014) Vinegoni et al. (2015) Swirski and Nahrendorf (2013)
Whole body optical imaging	s-min	~0.1 mm (organ) ~1 mm (body)	High sensitivity Many fluorescent markers available Relatively cheap	In most cases still 2D technique Requires genetically modified tumour cells Nude or shaved animals required	Alzheimer's disease Diabetes, Hypertension Osteoarthritis Tumour vasculature	Lin et al. (2014) Hall et al. (2012) Lai et al. (2004) Pesnel et al. (2012)

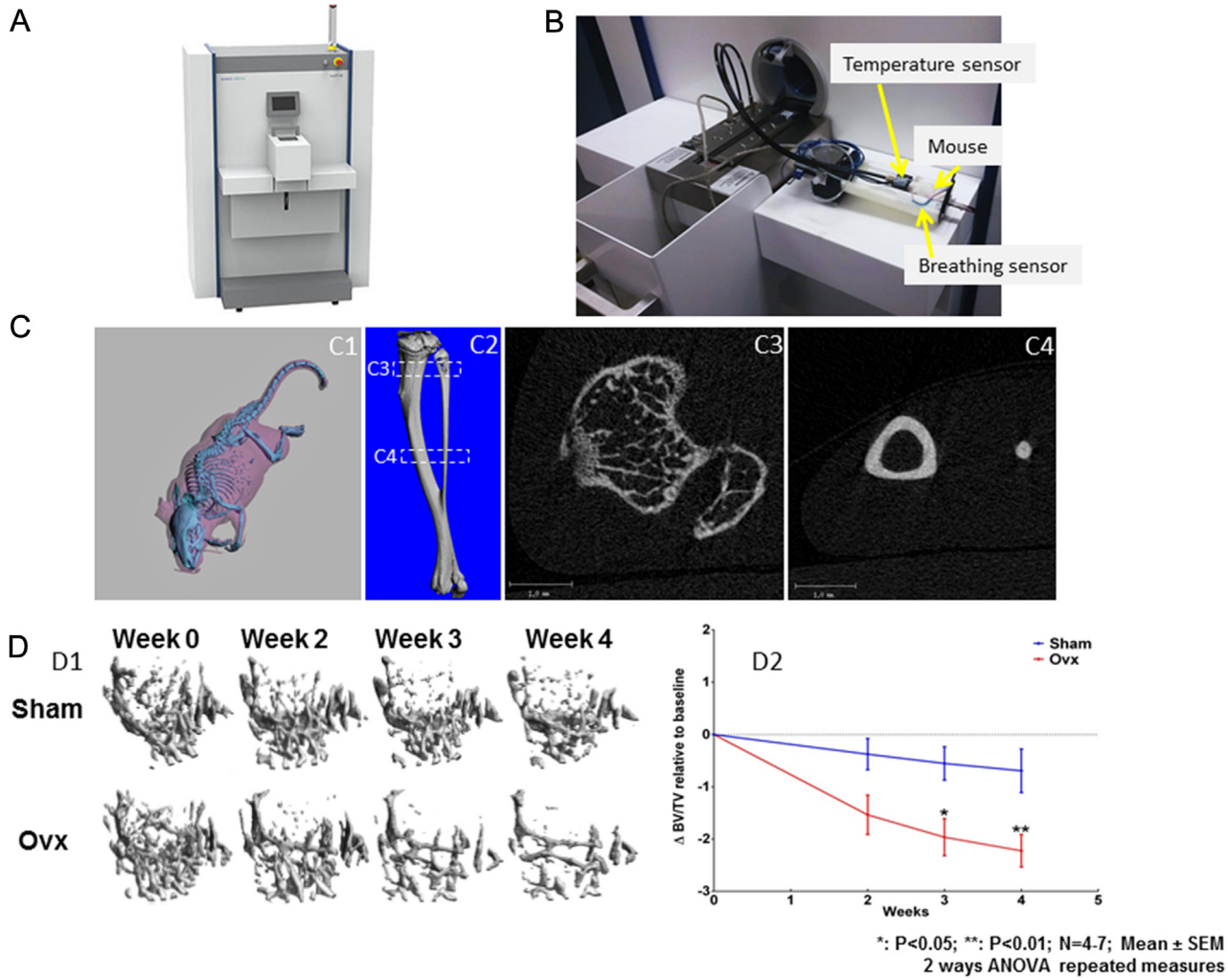

Fig. 1. Examples for *in vivo* micro-CT imaging: A) The Scanco Viva80 is an example of a commercially available *in vivo* micro-CT (courtesy of Scanco Medical AG). B) Particular of the scanning area and of the mouse holder with the sensors used to monitor the mouse status during the scan. Different images can be obtained with this system for analyses of bones: C1, low resolution scan and 3D reconstruction of the whole mouse skeleton and soft tissues. Scans were performed with 71.8 μm voxel size, 55 KeV voltage, 145 μA current, and 20 ms integration time; C2, high resolution scan and 3D reconstruction of the whole mouse tibia. Scans were performed with 10.4 μm voxel size, 55 KeV voltage, 145 μA current, and 200 ms integration time; C3-4, Cross sections of the reconstructed trabecular and cortical regions from C2. D: Example of analyses of longitudinal changes in trabecular bone volume fraction (BV/TV) with respect to baseline (week 0) with scans performed every week for ovariectomized (Ovx, N = 7) and sham operated (Sham, N = 4) 14 weeks old C57BL/6J female mice (unpublished data).

monary disease models when combined with respiratory gating (Artaechevarria et al., 2009; Johnson, 2007). This method can also be applied for monitoring the progression of lung tumours (Li et al., 2013; Rodt et al., 2009). Moreover, *in vivo* imaging of adipose tissue using micro-CT provides more details compared to 2D dual energy X-ray absorptiometry (DXA) and was found to be as accurate yet more cost and time effective than preclinical-MRI in assessing body composition and discriminating between adipose and non-adipose tissue (Luu et al., 2009; Wyatt et al., 2015). Another approach to visualize the target tissue is the use of contrast agents (Lusic and Grinstaff, 2013). For instance, *in vivo* contrast-enhanced micro-CT has been used to monitor liver tumours progression (Ohta et al., 2006), to evaluate rodent models of hepatic/brain ischemia and stroke (Hayasaka et al., 2012), to evaluate cartilage degeneration in rats (Piscaer et al., 2008), and to quantify vasculature in mice (Nebuloni et al., 2014; Starosolski et al., 2015). Finally, nanoparticles as contrast agents were used in an *in vivo* micro-CT setting to monitor tumour vasculature (Ghaghada et al., 2011), and the progression of lung tumours (Lalwani et al., 2013).

2.2.4. Summary of advantages and limitations

The main advantage of *in vivo* micro-CT imaging is the high penetration depth of X-rays through the different tissues, which leads to the high image resolution (voxel size down to 8–10 μm), enabling accurate longitudinal measurements of anatomical features, of bone or stained soft tissues. The great potential of *in vivo* micro-CT is also its ability to be coupled with other *in vivo* imaging modalities such as preclinical-PET in order to evaluate for example carcinogenesis and treatment strategies in circumscribed lung tumours (Rodt et al., 2009), and optical imaging to monitor for example the dynamic changes in bacterial burden, neutrophil recruitment and bone damage in a mouse orthopaedic implant infection model (Niska et al., 2012). More details about these techniques will be provided in the next sections.

Despite its advantages, *in vivo* micro-CT imaging has a number of limitations. First, being an X-ray based imaging modality; the associated radiation dose to which the animal is exposed during scanning is an important factor to consider as it could affect the measurements. Several studies have assessed the impact of successive imaging on the organ or tissue integrity and function.

It appears that the radiation affects differently soft and hard tissues and a number of studies have been performed to reach the best compromise between image quality and radiation dose (Klinck and Boyd, 2008; Laperre et al., 2011; Vande Velde et al., 2015). However, there is not yet general consensus about standardized scanning protocols for the different anatomical sites and there is no way to estimate the effective radiation dose (*i.e.* the tissue-weighted sum of the equivalent radiation dose in all tissues and organs of the body during the scan) in the mouse. Consequently, in order to reduce the scanning time and therefore the radiation dose, *in vivo* analyses are usually performed with lower resolution (9–15 μm for bone) compared to *ex vivo* imaging (down to 1–5 μm for bone), with a resulting decreased precision when measuring small features of mouse bones (*e.g.* average trabecular thickness in the proximal tibia is approximately 40–60 μm). A second limitation is related to motion artifacts: with micron level resolutions, any movement of the animal while under anaesthesia will lead to motion artifacts on the acquired images. To minimize them, special holders are provided by the manufacturers to ensure the target organ/tissue is well placed and maintained. However, they cannot be completely removed in particular when central sites (e.g vertebrae, lungs) are scanned. Additionally, animal wellbeing must be monitored at all times, increasing the complexity of the scan and the costs associated with it. Under general anaesthesia, mice are unable to maintain normothermia (with a drop in core temperature of 1 °C every 4 min for a C57Bl6 mouse) (Caro et al., 2013). It is therefore imperative to add a heating system in order to maintain the animal's temperature as close as possible to normothermia. Breathing pattern should also be monitored carefully, to minimize any discomfort to the animal, but also to minimize the risk of movement artifact (gasping, unsteady breathing pattern). When properly monitored, a mouse can be maintained under anaesthesia for up to 4 h, with fast recovery and no apparent short term effect (Lu et al., 2015a).

2.3. Preclinical magnetic resonance imaging (MRI)

2.3.1. Technique

Magnetic resonance imaging (MRI) utilises a strong magnetic field to polarise the magnetic moments of specific nuclei within the subject. This generates a significant equilibrium net magnetisation. Radio frequency coils are used to transmit short electromagnetic pulses to perturb this magnetisation. As the magnetisation relaxes back to the equilibrium position a decaying oscillatory electrical current is induced in the radio frequency antennae. To spatially localise the signal in three dimensions, powerful magnetic gradient coils are used to encode these oscillating signals in terms of their frequency and phase. These electrical signals are interpreted (*via* Fourier transform) into an image with different tissues having different signal amplitudes and decay rates. The amplitude of the signal is primarily affected by the nuclei density within the tissue. The decay rate is indicative of two different physical effects; i) the transfer of energy from the nuclear spin system to adjoining/lattice molecules and ii) the loss of phase of the oscillatory signal caused by magnetic field in-homogeneities and direct interaction between nuclei (without energy loss to the surrounding lattice). As such MRI has unparalleled soft tissue contrast and is now widely used in age related research in both human and animal studies. For a more detailed description of MR theory the reader should consult the existing literature [1–4].

Preclinical-MRI is an ideal technique for the investigation of several age related disease phenotypes; the main advantages being that it offers *in-vivo*, high resolution, 3D, non-invasive images. The latter importantly permits longitudinal studies using knockout and control mice, a prerequisite for advancing age related research. Furthermore, the preclinical-MRI technology used in the preclinical setting is identical to that already used in hospitals worldwide for diagnostic purposes but often provides smaller bore holes and higher magnetic field strength. This means that promising new *in vivo* biomarkers or treatment strategies involving preclinical-MRI, for age related disease phenotypes, have the potential for direct clinical translation.

2.3.2. Most common applications

The most commonly imaged nuclei in biological organisms are the hydrogen protons contained within the abundant water pool. The brain and heart (the most commonly imaged organs with MRI) are composed of 73% water. Other tissues that are associated with age related diseases, *e.g.* the muscles and kidneys are composed of 79% water (Mitchell et al., 1945). By imaging such tissues over time, development of solid organ atrophy and other phenotypes can be detected throughout the body. Since age is a major risk factor for neurodegenerative disease, MRI has been used extensively to monitor structural changes within the brain, comparing pathological measurements to normal age related changes.

Clinical MRI studies have shown that the brain decreases in total volume at an accelerated rate after the age of 50 (Craik and Salthouse, 2000; Raz et al., 2005; Raz and Rodrigue, 2006) and volumetric analyses with MRI is actively used in the diagnosis of mild cognitive impairment and Alzheimer's disease; with an impressive diagnostic accuracy of approximately 90% (Norfray and Provenzale, 2004). MRI technology has also shown that white matter changes are an effect of very old age (Raz et al., 2005; Salat et al., 1999; Sowell et al., 2003) whereas grey matter loss starts earlier and is more gradual.

These gross structural changes have been replicated in normal and transgenic mice used in ageing studies, using high field MRI (>7 T) that is commonly used in the pre-clinical setting (Maheswaran et al., 2009). Although simple structural MRI alone cannot define the causal pathway of these changes, it can help confirm that new mouse models of ageing and associated diseases are displaying the required pathology. Even though volumetric brain analysis appears to be a suitable metric of age related changes, the power of MRI really shines through when it is used in conjunction with other pre-clinical techniques. For example animal studies with electrophysiology and calcium dye imaging (Burke and Barnes, 2006) have provided evidence that deficit in brain plasticity (its ability to form new connections and memories) is a result of age induced changes in calcium regulation. Changes in calcium regulation directly affect action potentials as they traverse axons and thus change neuronal pathways. For a full review the reader is referred to Burke and Barnes (2006).

MRI also has the potential for identifying such breakdowns in cerebral networks directly, beyond measurements of gross structural deficits. Diffusion tensor imaging (DTI) gives a measure of the magnitude and orientation of the diffusion of water (the standard proton signal source). With no barriers, water is free to move in any direction, diffusing isotropically. However the brain is full of long neuronal bundles, which constrain the movement of the water so that it tends to follow the long axis of the bundles (resulting in anisotropic diffusion). DTI-MRI measures the strength of the directional dependence of diffusion and therefore to some extent tissue disruption, the so-called fractional anisotropy (FA). If the neuronal bundles are disrupted the molecular motion will return to its free diffusion state and lead to decreased FA. Studies using DTI-MRI FA metrics suggest that the microstructure of the white matter integrity is different between normal and pathological ageing (Minoshima and Cross, 2008; Song et al., 2004). However, like structural MRI there is no global standard for DTI analysis, which can drive over interpretation of results. It is in the end only measuring diffusion driven by axonal membrane integrity with myelin playing a modulatory role (Beaulieu, 2002).

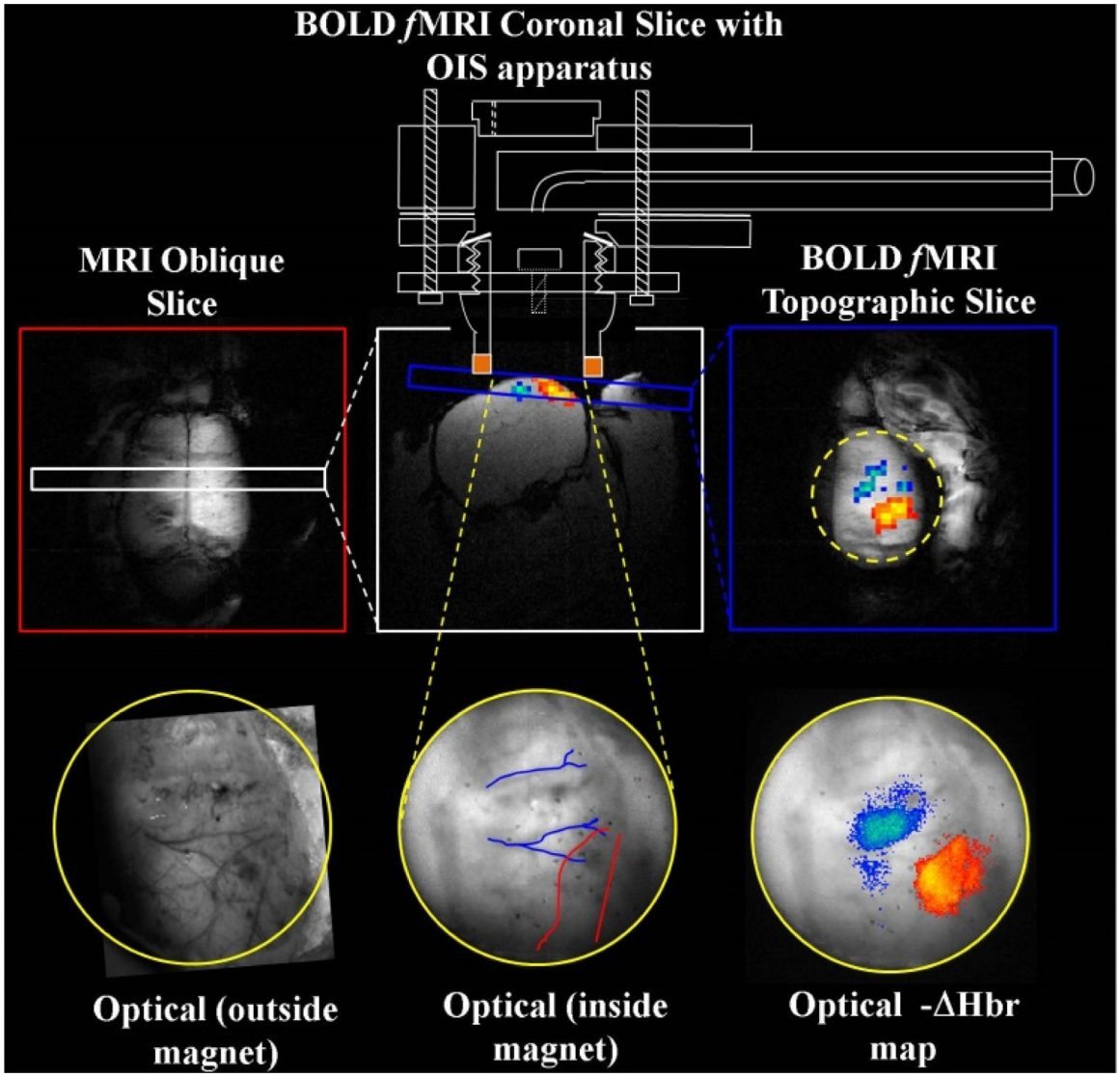

Fig. 2. BOLD fMRI is a very qualitative and pseudo measure of neuronal activity. Only by combing fMRI with other neuro-imaging techniques can one really understand neurovascular coupling. Concurrent fMRI and optical imaging can be used to investigate changes in the brain's vascular response with age in rats (Kennerley et al., 2012). BOLD fMRI statistical activation maps in this topographic plane can be compared directly to complementary functional haemodynamic statistical maps from 2D-OIS. The underlying micro-vasculature can be identified using optical imaging both inside the magnet and outside (without the endoscope).
Reproduced with permission from (Kennerley et al., 2012).

A surrogate measure of neuronal activity can be made using functional MRI (fMRI). fMRI relies on a process known as neurovascular coupling, where localised changes in neuronal activity drive changes in vessel diameter in order to control cerebral blood flow and to supply the required substrates to that region of the brain. The tissue is often hyper-perfused which leads to an overall increase in cerebral blood oxygenation, making the relative percentage of paramagnetic deoxyhaemoglobin lower. This homogenises the local magnetic field and results in an increase in MR signal magnitude – the so-called Blood Oxygenation Level Dependent (BOLD) fMRI signal (Kwong et al., 1992; Ogawa et al., 1990). Studies using this technique in rats have shown a change in the brain's vascular response with age (Dubeau et al., 2011). Subsequent breakdowns in neurovascular coupling can lead to decreased function (Sorond et al., 2011). BOLD fMRI by itself is a very qualitative measure and only a pseudo-measure of neuronal activity. In order to investigate if neuronal pathways break down and drive smaller changes in the haemodynamics or if the vascular disruption limits delivery of metabolites and cause cell death (Zlokovic, 2010), BOLD fMRI needs to be coupled with other neuro-imaging techniques such as optical imaging spectroscopy (Kennerley et al., 2012) (Fig. 2) and electrophysiology (Pan et al., 2010). This coupling provides measurements of changes in the haemodynamic response and neuronal response respectively in animal models.

Following the vascular hypothesis for neurovascular coupling breakdown as a mechanism of decreased cognitive function and development of neurodegenerative diseases, one could make a causal link from early age cerebral hypo-perfusion and vascular risk factors leading to white matter damage (Firbank et al., 2007; Spilt et al., 2005). Recent studies have attempted to elucidate the relationship between brain perfusion variability and risk factors of endothelial dysfunction and atherosclerosis in healthy aged subjects (Henriksen et al., 2014). It was concluded that the amino acid homocysteine, increased amounts of which make a person more prone to endothelial cell injury and thus blood vessel inflammation, may be a marker of cerebral perfusion in ageing brains. Magnetic

resonance angiograms, where stationary tissue contrast is nulled and only signal from flowing blood measured, could find use in the assessment of such effects (Beckmann et al., 2003; Slawson et al., 1998; Wiesmann et al., 2002, 2000).

Not only hydrogen nuclei in water but also nuclei in other molecules/metabolites exhibit magnetic resonance. This opens up the possibility of studying ageing effects on cellular metabolism in different organs. Importantly, the resonance frequency is different for each metabolite, which can therefore act as a finger-print of the relative concentrations of different target metabolites (Rudin, 1992), once the water signal is nulled. Magnetic resonance spectroscopy (MRS) predates MRI, and as an analytical technique has been applied to studies of ageing in human (Robertson et al., 2001) and in mice (Oberg et al., 2008; Yang et al., 2011). Moreover, Carbon-13 MRS can be used for characterising fluxes and pathways of metabolism. Using Phosphorus-31 MRS one can investigate adenosine tri-phosphate synthesis directly (Pettegrew et al., 1987). The problem is that these nuclei have low abundance in the body and therefore signals are difficult to measure. A new technique involving hyperpolarisation of carbon-13 labelled metabolic substrates, which can increase their MR signal by 10,000 times (Ardenkjaer-Larsen et al., 2003), has started a resurgence in the field of MRS. This technique has been used mainly for cancer research, but it has also been applied to investigate cardiac metabolism (Aquaro et al., 2013) – dysfunction of which is related to the ageing brain.

2.3.3. Summary of advantages and limitations

Preclinical-MRI is an ideal technique for the investigation of several age-related disease phenotypes; the main advantages being that it offers *in-vivo*, relatively high resolution, 3D, non-invasive images. The latter importantly permits longitudinal studies using knockout and control mice, a prerequisite for advancing age related research. Furthermore, this technique is very similar to its clinical counterpart, making the clinical translation straightforward.

Limitations of MRI are the inherent low sensitivity and, due to the size of the mouse compared to the human, the need for high field strength systems for pre-clinical studies. Most pre-clinical MRI centres employ MRI systems with field strengths of 7 T and above. The high field increases the nuclear magnetic polarisation and therefore the signal; in turn this can be sacrificed to increase the spatial resolution to achieve a good standard in the pre-clinical model. The small size of the mouse also necessitates the use of stronger imaging gradients (typically around 300+ mT/m in mice compared to 30+ mT/m in human) to enable to system to achieve these higher resolutions. In essence, both clinical and preclinical systems are superconducting solenoids surrounded by a helium cryostat. Preclinical systems only differ in their reduced bore size (to make the engineering of the higher fields and gradients easier). With this advanced/miniaturised technology comes a hefty price tag with pre-clinical MRI systems often on a par with their clinical counterparts. It might be naively presumed that the higher the field strength, the better for mouse imaging. However, although the polarisation (and hence signal) increases, the field becomes increasingly more difficult to homogenise (images appear distorted) and the relaxation times of the MR signal decrease with increased field strength. This means that image contrast changes and data must be captured in shorter echo time periods (Duyn, 2012). The choice of field strength must always be informed by the proposed application. For example, a reduced field strength is advised for imaging the pulmonary system to ensure relaxation times are long enough to capture data. For functional MRI, field strengths around 7–9.4 T are optimal for a balance between signal and image distortions with fast echo planar imaging. For these reasons, low field strength (<7 T) benchtop permanent magnet imaging systems are becoming common-place to complement high field superconducting systems. These are cheaper, smaller and do not require expensive cryogenics or cooling systems. For this reason, as this technique develops, one might see a separation of clinical and preclinical-MRI techniques – whether this be an advantage or disadvantage remains to be seen. There are also other limitations related to the handling of living animals during the scanning protocol, especially within the very small bores of high field strength systems. The animal is usually anaesthetised by using gaseous isoflurane, levels of which are incredibly difficult to stabilise when all monitoring equipment has to be non-magnetic and by necessity is viewed remotely outside the scanner room. Breathing rate is often the only metric one has to assess the levels and this can change rapidly in a mouse. It can also be a challenge to keep the animals warm within the cold bore of a superconducting magnet. Different centres have very different strategies, employing hot air, heating blankets or water based systems, sometimes without temperature control feedback. Any slight changes in basic physiology (which could also be different between knockout groups and controls) could be a major contributing factor in result variation and can be incredibly to control for. Schneider et al. (2008) attempted to use cine-MRI for determining global cardiac function longitudinally in guanidinoacetate *N*-methyltransferase (GAMT) knockout, and wild type littermate mice. They soundly hypothesized that lack of creatine in GAMT knockouts would be detrimental for resting cardiac performance during ageing. However, they found no physiologically significant differences in cardiac function between wild type and GAMT knockout mice at any time point, perhaps reflecting some comprehensive adaptation in the knockouts to account for lack of creatine or again that changes in physiology masked the results. Although perhaps a perplexing negative result, the study was the first to report on the longitudinal investigation of a transgenic mouse model using cardiac MRI over the period of one year. This application demonstrates the power of the technique to accurately quantify cardiac functional parameters in genetically modified mice in a longitudinal fashion and start to address the link between cardiac and brain ageing.

2.4. Preclinical positron emission tomography (preclinical-PET)

2.4.1. Technique

Positron emission tomography (PET) can visualize the distribution and concentration of radiolabelled molecules injected into the subject and can be used to monitor, *in vivo*, biological processes such as enzymatic reactions, cellular metabolism, cell proliferation and migration (Phelps, 2000). Its preclinical version is a potent imaging modality for the investigation of age related diseases *in vivo* in mouse models. PET offers a high sensitivity and specificity for most imaging applications.

The spatial resolution of preclinical PET systems should ideally compensate for the smaller organ sizes in mouse models compared to humans. Thanks to advances in light detector technology, systems with spatial resolutions in the order of 1.5 mm to 1.6 mm (Balcerzyk et al., 2009; Bao et al., 2009) and below, some resolving structures smaller than 1 mm in size (Bergeron et al., 2014; Nagy et al., 2013), are now commercially available. It is even possible to resolve structures as small as 0.7–0.8 mm using some research systems (España et al., 2014; Weissler et al., 2015). However, this is still a relatively low resolution when considering the small size of mice. Unfortunately, time-of-flight PET (ToF-PET) does not significantly improve the image quality of preclinical imaging directly, but a good timing resolution still allows users to reduce the random coincidences rate (Strother et al., 1990). Recently, ToF-PET benefits were imaged for phantom diameters equivalent to the size of a rabbit on a research system with a timing resolution of about 260 ps but could not be shown for mouse-sized activity distributions (Schug

et al., 2015a), that would need a further improvement of timing resolution (below 100 ps).

As most PET tracers only allow acquisition of functional information, PET is often combined with a second imaging modality to provide an anatomical reference image. The combination of PET and computed tomography (CT) is commonly used in clinics as well as for preclinical applications. Here, the two modalities image the subject sequentially and not at the same time (Fig. 3A). PET integrated into an MRI system, on the other hand, offers real simultaneous image acquisition allowing for excellent spatial as well as temporal co-registration if the interference between the two modalities can be reduced to an acceptable level (Schug et al., 2015b; Wehner et al., 2015; Weissler et al., 2015) (Fig. 3B).

Many age related diseases can be studied with the help of mouse models. We discuss a few of the most common diseases with focus on the PET imaging possibilities and challenges. Examples of prominent diseases are picked from the fields of neurodegenerative, cardiovascular, and metabolic diseases and cancer without claiming to give a full overview.

2.4.2. Neurodegenerative diseases

Dementia is a disease strongly related to ageing with Alzheimer's disease (AD) being the most common form. The pathological features in the AD brain include amyloid-β (Aβ) plaques which can be imaged with PET (Nordberg, 2004). An established method for *in vivo* evaluation of Aβ-plaque burden in the human brain is PET using the Pittsburgh compound-B (PiB) (Ikonomovic et al., 2008; Klunk et al., 2004). Recent technical improvements in preclinical PET systems allowed a successful translation to mouse models, including a gain in spatial resolution (Manook et al., 2012) (Fig. 3C). Besides imaging of Aβ plaques, tau is a further promising target in early AD diagnosis. Neurofibrillary tangles are primary markers of AD and represent aggregates of the hyperphosphorylated tau protein. A novel tau-targeting PET radiotracer is [^{18}F]THK523 has shown very promising results in preclinical (Fodero-Tavoletti et al., 2011) and clinical studies (Okamura et al., 2014).

Parkinson's disease (PD) is another common neurodegenerative disorder related to ageing, mainly affecting the motor system. In later stages of the disease, thinking and behavioural problems may arise. PD has been investigated in toxin-induced and genetic models (Bové et al., 2005; Fleming et al., 2005; Melrose et al., 2006). Using recent preclinical PET systems it has become feasible to study PD using [^{18}F]DOPA *in vivo* in *e.g.* weaver mutant mice (Sharma and Ebadi, 2005; Waerzeggers et al., 2010).

In general, for detailed investigations of neurological activity and diseases using preclinical PET the spatial resolution of the image is a crucial performance parameter. With state-of-the-art systems it is possible to resolve individual regions of the mouse brain which enables *e.g.* the imaging of changes in brain activity using [^{18}F]fluorodeoxyglucose (FDG).

For multimodal imaging of neurodegenerative diseases, preclinical-PET and preclinical-MRI is the preferred combination because preclinical-MRI provides an anatomic reference image with excellent soft-tissue contrast to morphologically describe the pathologic alterations and also allows measuring their impact on neuronal activity and connectivity (Jack et al., 2010; Logothetis et al., 2001).

2.4.3. Cardiovascular diseases

Atherosclerosis is a chronic age related disease that remains asymptomatic for decades and is the principal cause of heart attack, stroke and gangrene of the extremities and responsible for 50% of all mortality in the USA, Europe and Japan (Ross, 1993). It is often caused by high-risk plaques whose features may show a thin fibrous cap, large necrotic core, macrophage infiltration, neovascularization, and intraplaque hemorrhage (Owen et al., 2011). In the clinic, several of these features can be investigated using PET. For example, FDG is often used to identify inflammatory plaques rich in macrophages (Rudd et al., 2002; Tawakol et al., 2006).

A wide range of animal models for atherosclerosis research is available (Kapourchali et al., 2014). In general, they are most useful to investigate the aforementioned features of plaques but not so much to model the complications of atherosclerosis, such as rupture and thrombosis (Cullen et al., 2003). While FDG PET was used to study atherosclerosis in rabbits (Nie et al., 2016) in order to predict plaque rupture (Aziz et al., 2008), mice have to be genetically modified in order to develop atherosclerosis at all because of a very different fat metabolism. Most common is the transgenic ApoE deficient mouse model, where mice develop plaques in dependence of their diet. In this model plaque rupture can be triggered by surgical ligation of the brachiocephalic or carotid artery (Hartwig et al., 2015; Matoba et al., 2013). Using ApoE deficient mice, it could be shown that FDG-PET is able to distinguish shear-stress induced, inflamed atherosclerotic plaques from non-inflamed plaques *in vivo* (Cheng et al., 2006; Wenning et al., 2014). An even more accurate characterization of the inflammation status in plaques may be enabled using, amongst others, the macrophage targeted probes [^{64}Cu]TNP (Nahrendorf et al., 2008) or (LyP-1)$_4$-dendrimer-^{64}Cu (Seo et al., 2014), the scavenger receptor targeted probe ^{64}Cu-CD68-Fc (Bigalke et al., 2014), ^{64}Cu-DOTA-vMIP-II binding to viral macrophage inflammatory protein II (vMIP-II) (Liu et al., 2013) and the $\alpha_{v\beta3}$ integrin-targeted tracer ^{18}F-galacto-RGD (Laitinen et al., 2009; Saraste et al., 2012).

2.4.4. Metabolic diseases

Diabetes mellitus (DM) type 1 is caused by a loss of the insulin-producing β-cells, which are found in the pancreatic islets. DM type 2 on the other hand is characterized by insulin resistance. PET is often used to image the β-cell mass and number which is challenging in mice *in vivo* because of the small dimensions of the pancreas and the spotted location and considerably low number of pancreatic islets. Furthermore, the pancreas is located close to the kidney, which is the excretion organ of most PET probes. Therefore, there is high demand for high spatial resolution to separate signals from both organs. Nonetheless, PET imaging using [^{18}F]fluorohydroxymethyl-butyl-guanine (FHBG) is sensitive to changes in β-cell mass that precede the onset of diabetes (McGirr et al., 2011). This has been shown in mouse models of diabetes type 1 and type 2 expressing multi-modality reporters for fluorescence microscopy and *in vivo* bioluminescence imaging in their β-cells. These models nicely confirmed that the FHBG PET signal strongly correlates with the β-cell number and mass (Yong et al., 2011).

2.4.5. Tumours

The most frequent deadly disease related to ageing is cancer. With a higher age of the patient or animal, increasing instability of the genome, decreased activity of the immune system and accumulated environmental influences lead to a higher probability of developing tumours.

As a quantitative whole body imaging modality and due to the availability of excellent radiotracers PET is ideally suited for the imaging of cancer, both for clinical and preclinical applications (Gambhir, 2002). Multiple tracers have been used to study glucose metabolism ([^{18}F]FDG), amino acid ([^{11}C]methionine) and choline ([^{11}C]choline) uptake, cell proliferation ([^{18}F]FLT), inflammation ([^{18}F]Galacto-RGD) and hypoxia ([^{18}F]MISO). Among those FDG is the most widely used radiotracer, because it is readily available and has been shown to work effectively due to the high glucose consumption of most malignant tumour cells (Vander Heiden et al., 2009). Besides these purely diagnostic radiotracers targeting

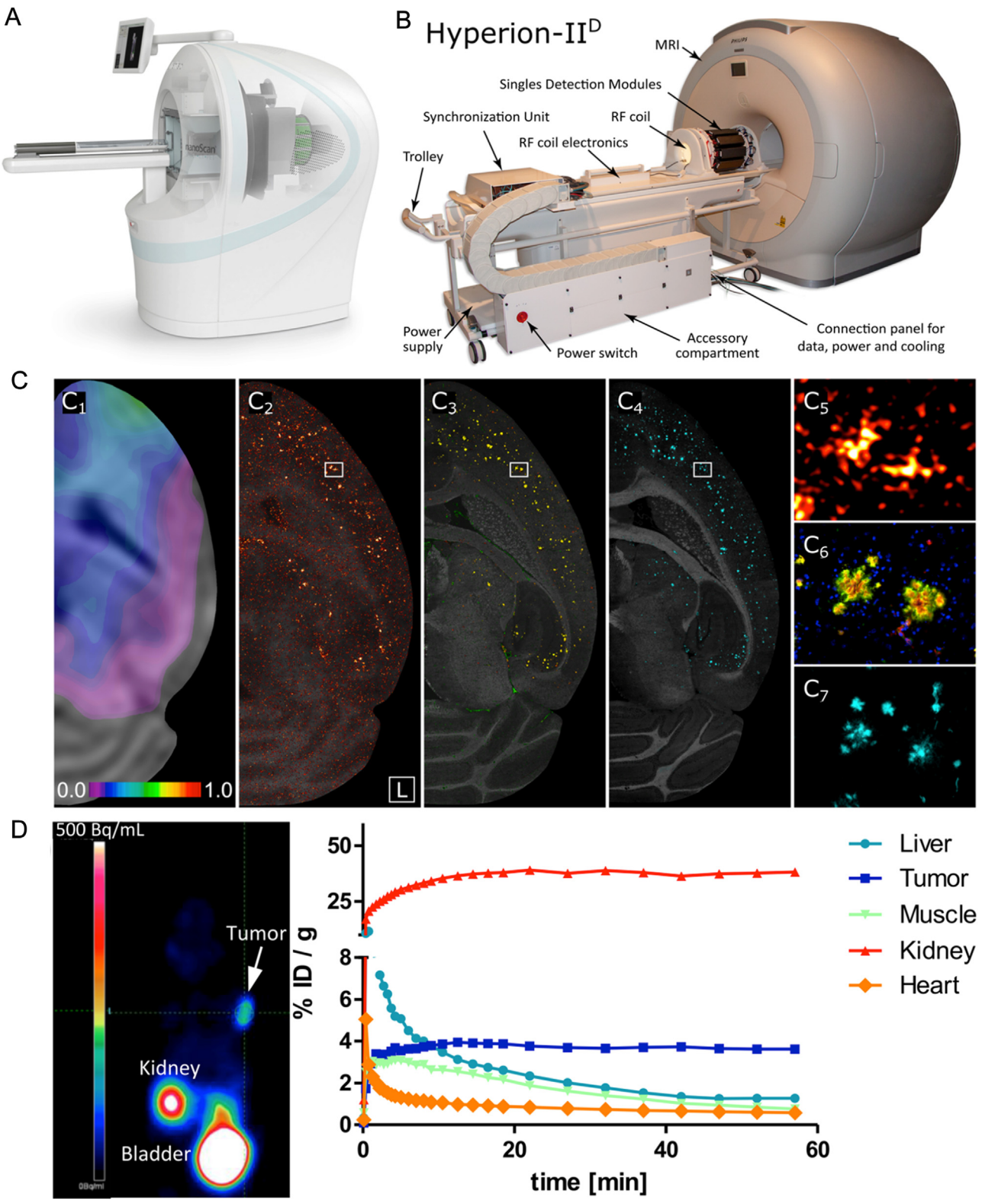

Fig. 3. Examples for preclinical hybrid PET imaging devices are shown in A and B:.
A: The nanoScan® SPECT/CT/PET is an example of a commercially available multi-modality preclinical imaging device (©MEDISO Medical Imaging Systems, courtesy of MEDISO).
B: The PET/MRI research insert "Hyperion-IID" is shown mounted on a standard patient table of a clinical 3T MRI system (gantry cover removed). The system allows real simultaneous image acquisition with both modalities (Adapted and reprinted from (Weissler et al., 2015)). Examples for PET imaging of mice with neurodegenerative and oncologic diseases are shown in C and D:
C: Alzheimer's disease imaging in a mouse showing Aβ-positive plaques *in vivo* and *ex vivo*. PET images are acquired with the tracer [^{11}C]PiB. Corresponding autoradiography and fluorescence microscopy images confirm PiB binding to plaque sites.
C1: [^{11}C]PiB PET image. The low resolution of PET does not allow identification of individual plaque sites but larger affected brain regions can be seen. The width of color scale represents 3 mm in reality.

more general tumour mechanisms, there are radiotracers which are very closely linked to therapy and act as companion diagnostics and theranostics. For example, the majority of lung cancers are non-small-cell lung cancers (NSCLC) which are difficult to treat. A small subset of NSCLC express mutations of the epidermal growth factor receptor (EGFR), which are sensitive to tyrosine kinase inhibitors, such as erlotinib (Wu et al., 2012). Thus, there is a demand for methods to select these patients for erlotinib therapy and to exclude those who do not express EGFR. This is an excellent example for the indication of personalized therapy and a motivation to develop companion diagnostics and theranostics. In this context, the PET tracer [^{11}C]-erlotinib was developed and successfully evaluated in mouse models of lung cancer overexpressing EGFR (Li et al., 2007; Memon et al., 2009). However, in mouse models the strong accumulation of [^{11}C]-erlotinib in the liver sometimes made it difficult to identify basal lung cancer signals due to spillover effects especially on PET systems with a low spatial resolution. As another example, older age is one of the main risk factors for prostate cancer. A wide range of mouse models is used in prostate cancer research including xenograft and transgenic mouse models (Ittmann et al., 2013). For visualization with PET, an ^{18}F-labeled choline analogue ([^{18}F]fluoromethyl-dimethyl-2-hydroxyethyl-ammonium (FCH)) was successfully applied both in humans and mouse models (DeGrado et al., 2000). Even better results were obtained with recent PET-radiotracers targeting prostate specific membrane antigen (PSMA). Of those ^{68}Ga-labelled PSMA showed excellent binding properties in mice bearing LNCaP tumour xenograft (Schäfer et al., 2012) (Fig. 3D) as well as in humans where it proved to be superior to choline tracers (Afshar-Oromieh et al., 2014). A further advantage of this compound is that ^{68}Ga can be replaced by the therapeutic radioisotope ^{177}Lu and initial results in tumour bearing mice as well as in patients show promising therapeutic outcomes (Kratochwil et al., 2015).

2.4.6. Summary of advantages and limitations

Preclinical-PET imaging of mouse models is highly valuable for the investigation of age related diseases as it offers high sensitivity, specificity and a wide range of available tracers for various disease fields as for example neurodegenerative, cardiovascular, and metabolic diseases and cancer (see Table 2 for a selective overview).

The limiting factor of investigating mice with PET is, besides the high cost and the handling with (sometimes fast decaying) radioactive material, mainly the low spatial resolution which, however, has seen constant improvement over the last years. In addition, its limitations in anatomical information can be compensated by hybridizing PET with CT or MRI. Finally, animal handling has a big impact on the metabolism of a mouse and FDG performed in liver, brain and other organs can strongly vary dependent on the metabolic state, activity and temperature of the animal. Anaesthesia of animals should also be considered. Isoflurane is well suited for tumour-bearing mice. Ketamine/xylazine, on the other hand, may induce hyperglycemia (Fueger et al., 2006).

2.5. Preclinical single photon emission computed tomography (preclinical-SPECT)

2.5.1. Technique

Single Photon Emission Computed Tomography (SPECT) detects gamma radiation that is directly emitted by a radionuclide during decay. SPECT is similar to conventional nuclear medicine planar imaging by a gamma camera, but is able to provide 3D information by acquiring multiple 2D-images while rotating around the imaged object.

Due to the physical principle of SPECT-imaging, it is necessary to implement collimators in SPECT-scanner systems to gain spatial information of the gamma decay. Collimators absorb photons that are not within a small angular range. For small animal research pinhole or multiple-pinhole collimators are usually used (Van Audenhaege et al., 2015), which provide a high spatial resolution (preclinical-SPECT). Resolutions <1 mm can be achieved by replacing clinical standard collimators (resolution 6–8 mm), such as parallel-hole, fan-beam and cone-beam collimators, with a pinhole collimator (Acton and Kung, 2003).

2.5.2. Applications

SPECT has a wide range of applications due to different available tracers and, therefore, offers many options to image the ageing mouse. The main ageing-related applications are myocardial perfusion, neurodegenerative diseases, oncology and bone metabolism.

The risk of a myocardial infarction increases with age. Using ^{99m}Tc-Sestamibi Wollenweber et al. (2010) showed the ability of cardiac perfusion preclinical-SPECT to detect myocardial perfusion defects in mice. The infarct volumes measured by SPECT correlated highly with the results of gold-standard histology. Furthermore, transgenic mice with overexpression of the EP3 receptor leading to cardiac hypertrophy showed a lower cardiac uptake of ^{99m}Tc-Sestamibi compared to wild type mice (Pissarek et al., 2009). Further tracers for measuring cardiac function are ^{99m}Tc-TETRO (Vrachimis et al., 2012) and ^{123}I MIBG (Dimitriu-Leen et al., 2015).

Neurodegenerative diseases, such as Parkinson's disease and Alzheimer's disease, and other forms of dementia can also be evaluated with preclinical SPECT. Several SPECT-tracers are available to image Parkinson's disease: ^{99m}Tc-TRODAT-1 and ^{123}I FP-CIT bind to dopamine transporters (DAT), which in healthy people and mice are strongly expressed in striatum and reduced in this disease (Hwang et al., 2002). Accurate detection of losses of approximately 60–80% striatal DAT after injection of 1-methyl-4-phenyl-1,2,3,6-tetrahydropyridine (MPTP) was found using the tracer ^{123}I FP-CIT (Andringa et al., 2005). However, the tracer did not permit an accurate evaluation of the nigral dopaminergic cells in Parkinson's disease (Alvarez-Fischer et al., 2007). To differentiate between idiopathic Parkinson's syndrome and atypical Parkinson's syndromes (multiple system atrophy, progressive supranuclear palsy), the dopamine D2 receptor ligand ^{123}I IBZM is used in clinical routine (Heinzel et al., 2015). ^{123}I IBZM is also an appropriate tracer for D2-receptor SPECT in healthy mice (Meyer et al., 2008; Pissarek et al., 2009).

C2: Digital [^{3}H]PiB *ex vivo* autoradiograph showing the PiB binding sites in high-resolution which allows to distinguish individual plaque sites. The Aβ burden is visualized with double immunofluorescence microscopy of Aβ40 (green) and Aβ42 (red) in C3 and with thioflavin S fluorescence (FITC excitation, cyan) in C4.
C5–7: Identical Aβ plaque constellations of adjacent sections as marked by white rectangle in C1–3. C5: magnification of digital autoradiograph as seen in C2. C6: corresponding magnified view of Aβ40/Aβ42 stain as seen in C3. C7: Corresponding magnified view of Thioflavin S stain as seen in C4.
The comparison of the PiB image nicely matches the fluorescence images indicating the specific binding of PiB (Adapted and reprinted from (Manook et al., 2012)).
D: PET imaging of a prostate cancer mouse model using a PSMA targeting tracer. After a dynamic preclinical-PET scan, a static scan was performed 1 h post-injection. The whole-body coronal preclinical-PET image of an athymic male nude mouse bearing an LNCaP tumour xenograft enables clear identification of the prostate tumour site with the kidney and bladder showing strong signals as well. The graph showing organ activity as a function of time demonstrates the excretion of the tracer by the kidney, its elimination from most organs and the persistent accumulation in the tumour. After 1 h the heart, muscle and liver background is reduced, which allows measurement of a clear tumour signal. Thus, optimal timing (or even better kinetic analysis) is required to distinguish passive accumulation from active target binding (Adapted and reprinted from (Schäfer et al., 2012)).

Table 2
Selection of PET tracers used in clinical and preclinical applications.

Nuclide	Tracer	Fields of use
^{11}C	[^{11}C]choline	Prostate cancer diagnosis (alternative: [^{18}F]FCH)
	[^{11}C]PiB	Aβ plaque burden; Alzheimer's disease
	[^{11}C]methionine	Amino acid transport; brain tumour diagnosis
	[^{11}C]Acetate	Oxidative metabolism, fatty acid metabolism
^{15}O	$^{15}O_2$ [^{15}O]Water	Oxygen intake and distribution Perfusion imaging
^{18}F	[^{18}F]FDG	Glucose utilization; tumours, brain activity, inflammation (plaques)
	[^{18}F]FCH	Prostate cancer diagnosis
	[^{18}F]FLT	Cell proliferation; cancer diagnosis
	[^{18}F]MISO	Hypoxia
	[^{18}F]DOPA	Presynaptic dopaminergic integrity; Parkinson's disease
	[^{18}F]THK523	tau targeting; Alzheimer's disease
	[^{18}F]FHBG	β-cell imaging, Diabetes
	[^{18}F]Galacto-RGD	Angiogenesis, inflammation; tumours, cardiovascular diseases,
	[^{18}F]NaF	tumour metastasis and angiogenesis ($\alpha\nu\beta3$ expression) Bone mineralization
^{68}Ga	[^{68}Ga]PSMA	Prostate cancer diagnosis

Dementia affects app. 40 million people, mostly older than 60 years, worldwide (Scheltens et al., 2016). Alzheimer's disease is the most common form of dementia, followed by vascular dementia and dementia with Lewy bodies. In this context, DAT-SPECT with ^{123}I FP-CIT seems to be an ideal method to accurately distinguish between these pathologies (Shimizu et al., 2016). ^{99m}Tc-HMPAO-SPECT is used in clinical practice to measure cerebral perfusion (Heiss, 2014). However, it is also a promising technique for measuring rCBF (regional cerebral blood flow) in preclinical research (Apostolova et al., 2012) and has been shown to depict age-related changes during late maturation (juvenile and young adult) in mice. In contrast, ^{99m}Tc-ECD, another clinical tracer for cerebral perfusion, is more difficult to be applied in mouse-brain SPECT because of its fast tissue clearance (Apostolova et al., 2012).

In oncology, SPECT is frequently used to image neuroendocrine tumors (NET) by using ^{111}In-octreotide, and [^{177}Lu-DOTA-Tyr3]-octreotate for the visualization of somatostatin receptors (Bison et al., 2015; Ullrich et al., 2016), to image thyroid cancer pre- and post-therapeutically using ^{123}I/^{131}I-NaI (Liu et al., 2011; van der Have et al., 2016) and to perform bone scintigraphy. For the latter, the tracer ^{99m}Tc-MDP is used, which characterizes bone metabolism in both degenerative changes and cancer (Cowey et al., 2007; Lienemann et al., 2015). Multiple further tracers such as ^{111}In-cCPE-GST, which binds to Claudin 4, that is overexpressed in several premalignant precursor lesions are available (Mosley et al., 2015), but it would go over the scope of the article to provide a complete overview (Bernsen et al., 2014; Cai and Li, 2013; Franc et al., 2008).

2.5.3. Summary of advantages and limitations

The main advantage of SPECT is that it is less cumbersome and less expensive than PET. A wide range of tracers can be used for both of these imaging modalities to visualize different functional information. SPECT even offers the possibility of imaging multiple radio-labelled probes simultaneously. Energy discrimination can be performed to differentiate between different radioisotopes emitting gamma rays at different energies. Many radionuclides used for SPECT imaging can either be eluted from generator-systems or due to their intermediate half-lifes produced in large amounts and distributed by pharmaceutical companies. Even though SPECT does not provide morphological information, it can be combined with CT (SPECT-CT) or MRI (SPECT-MRI) (Franc et al., 2008).

On the downside, SPECT has a reduced (10 times lower (Sandhu et al., 2010)) sensitivity compared to PET in both clinical and preclinical settings (Rowland and Cherry, 2008), because lots of radiation is lost in absorptive collimation. Furthermore, radiation exposure cannot be disregarded, which is particularly critical for long-term observations of mouse models of ageing.

2.6. Ultrasound

2.6.1. Technique

Ultrasound is a mechanical wave operating usually between 2–30 MHz. Because ultrasound is a mechanical wave, there is no ionizing radiation involved during the imaging of mice. During the imaging procedure, the animals are lightly anesthetized with 1% isoflurane and in order to provide optimal ultrasound penetration the hair is removed with a topical depilatory agent. The ultrasound transducer is usually fixed in a positioning device and acoustic coupling through gel is made to the mouse. High-frequency ultrasound transducers produce high-resolution images of small structures, ideal for detecting organ pathology in mice. The role of ultrasound imaging in the ageing mouse lies mostly in cardiac applications (Kepez et al., 2008; Ram et al., 2011) (Fig. 4). However, it has recently been shown (Springer et al., 2014) to have a role in assessing kidney pathology in mouse models.

2.6.2. Cardiac applications

Typical measurements provided by echocardiography in mice include chamber dimensions, wall thickness, and ejection fraction (EF). These measurements are useful because one can determine functional changes in the heart caused by myocardial injury, genetic modifications disease, drug treatments, and ageing (Ram et al., 2011). Recently, myocardial strain measurements (Abraham et al., 2007; Derumeaux et al., 2008; Friedberg and Mertens, 2013; Springer et al., 2014) have been utilized to evaluate regional left ventricular abnormalities that are not normally explored with conventional echocardiographic measurements.

The goal of the study performed by Rosenblatt-Velin et al. (2012) was to use stem cell antigen-1 (Sca-1) in order to identify cardiac stem cells in the mouse heart using transthoracic echocardiographies, by using a 30-MHz transducer. In order to investigate the function of the antigen in ageing and during the cardiac adaptation to stress, Sca-1-deficient mice were used. These mice developed consistently dilated cardiomyopathy. Furthermore, the hearts of mice lacking Sca-1 demonstrated exacerbated susceptibility to pressure overload. The heart was imaged in the 2D mode in the parasternal long-axis view. From this view, M-mode ultrasound was obtained measuring left ventricle (LV) free wall thickness in

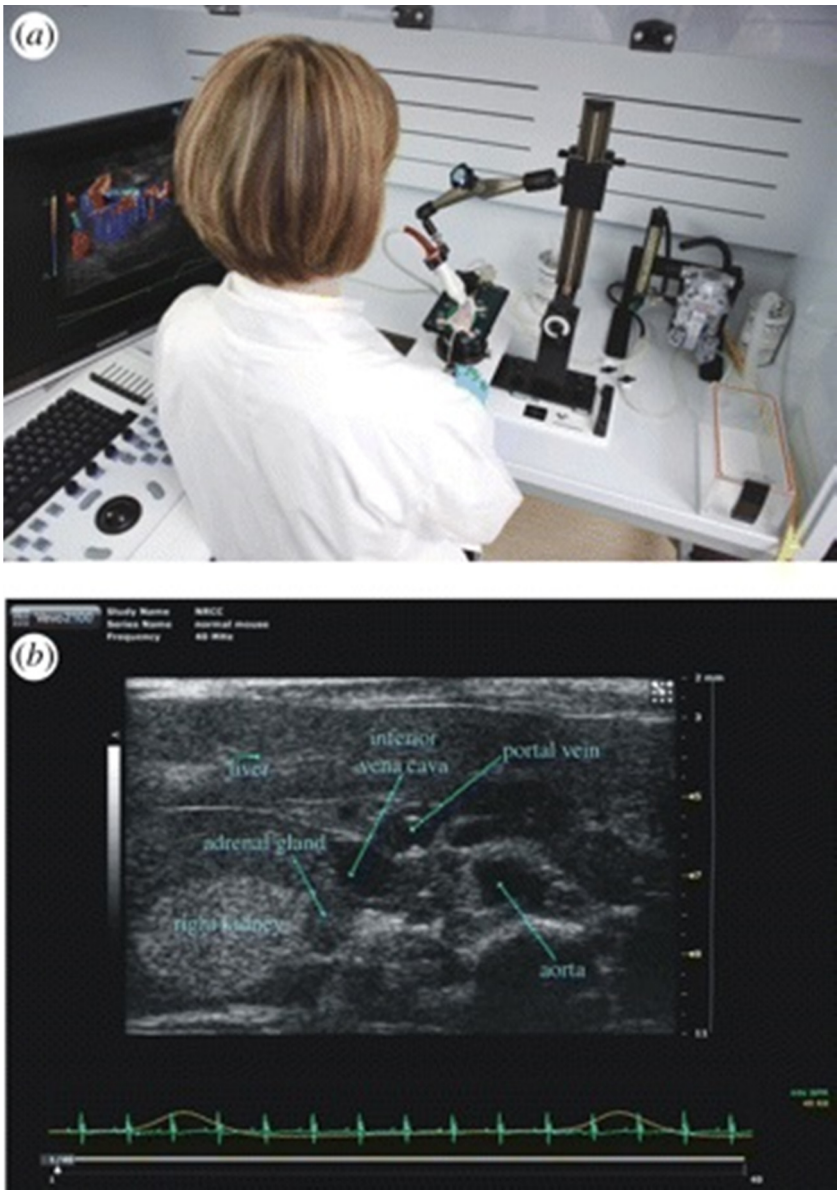

Fig. 4. Examples for preclinical US imaging setup (a) and an example of US image of abdominal imaging in mice (b).

diastole and in systole as well as LV diameter in diastole and in systole.

The natural ageing process results in the physiological decline of multiple tissues and organ systems including the heart. Changes commonly occur with middle age includes among others heart failure. Recent studies by Jackson et al. (2012) suggest that myostatin may influence cardiac output. In this study an 18 MHz linear epicardial transducer was used, while a 10 MHz-phased array transducer was used for strain acquisition. Echocardiography was performed on anesthetized mice in order to assess basal and maximal cardiac performance using isoproterenol stress tests, which cannot be performed on non-anesthetized mice as handling these mice induces a stress response. Standard imaging planes, M-mode, Doppler, and functional calculations were obtained. The left ventricle (LV) parasternal long axis four-chamber view was used to derive ejection fraction (EF) as well as ventricular dimensions and volumes. The left parasternal short axis view was used to obtain M-mode ventricular wall measures, fractional shortening (FS), and for radial strain analysis. Finally, the subcostal long axis view, from the left apex, was used for Doppler imaging of mitral inflow and aortic ejection profiles. Stress tests were performed after first obtaining a baseline echocardiogram followed by i.p. injections of isoproterenol (10 mg/kg).

The commonly used anaesthetic agent, isoflurane, is a potent coronary vasodilator which could potentially be used in the assessment of coronary reserve, but its effects on coronary blood flow in mice are unknown. Coronary reserve is reduced by age, coronary artery disease, and other cardiac pathologies. In the study by Hartley et al. (2007) Doppler ultrasound was used to measure coronary flow velocity in mice anesthetized at low (1%) and at high (2.5%) levels of isoflurane to generate baseline (B) and elevated hyperemic (H) coronary flows respectively. A 20 MHz Doppler probe was utilized transthoracically toward the origin of the left main coronary arteries of six weeks, two years, and two years apolipoprotein-E null (ApoE−/−) atherosclerotic mice. It was concluded that Doppler ultrasound combined with coronary vasodilation *via* isoflurane could provide a convenient and non-invasive method to estimate coronary reserve in mice, but also that care must be taken when assessing coronary flow in mice under

isoflurane anaesthesia because of its potent coronary vasodilator properties.

Tomita et al. (2012) established the relationship between hemodynamics and atherosclerosis in aortic arches of ApoE−/− mice. Mean flow velocities at the ascending and descending aorta (mVAA and mVDA) were measured by Doppler ultrasound in wild type and ApoE−/− male mice at three and nine months of age.

Another example of the use of ultrasonic imaging of cardiac function was proposed by Zhou et al. (2012). In their study, they reported mitochondrial oxidative stress over a lifetime and concluded that it causes aortic stiffening by inducing vascular wall remodeling, intrinsic changes in smooth muscle cell (SMC) stiffness and aortic SMC apoptosis (Zhou et al., 2012). Pulse wave velocity in the heart was measured using Doppler with a 30 MHz probe.

The study by Halade et al. (2011) suggested that rosiglitazone RSG treatment has context dependent effects on cardiac remodeling and serves a negative cardiac role when given with a corn oil enriched diet. Mice were lightly anesthetized with isoflurane (0.5–2%) and 2D targeted M-mode echocardiographic recordings were obtained. Dimensions and wall thickness of the LV were measured and fractional shortening was calculated.

Dopamine D3 receptor has a critical role in the emergence of age related cardiac fibrosis, remodeling, and dysfunction (Johnson et al., 2013). Animals underwent high-resolution echocardiography using a 30 MHz transducer, in experiment to assess the role of Dopamine D3 on cardiac fibrosis.

2.6.3. Other applications

Ultrasound imaging plays a role in kidney assessment of ageing mice (Springer et al., 2014). Using a 40 MHz linear array transducer, high-resolution images were obtained in a diversity of pathologic lesions occurring within the abdomen of geriatric mice with acquired hydronephrosis (Springer et al., 2014) that enabled a determination of the underlying aetiology. Aetiologies diagnosed from the imaging results include pyelonephritis, neoplasia, urolithiasis, mouse urologic syndrome, and spontaneous hydronephrosis, and were confirmed at necropsy. This report highlights the utility of high-frequency ultrasound for surveying research mice for age-related pathology, and is the first comprehensive report of multiple cases of acquired hydronephrosis in mice. Moreover, it was recently demonstrated that preclinical high-frequency US can be used to study the development of nonalcoholic fatty liver disease (NAFLD) in mice, with also potential therapeutic implications (Fernandez-Dominguez et al., 2011).

2.6.4. Summary of advantages and limitations

The main advantages of ultrasound are: a) there is no ionizing radiation involved, b) it is the fastest imaging modality, c) the cost of purchasing and operating the device is the lowest, d) it is portable, and e) easy to use. Echocardiography is a robust tool for assessing cardiac (Abraham et al., 2007; Derumeaux et al., 2008; Friedberg and Mertens, 2013; Halade et al., 2011; Hartley et al., 2007; Jackson et al., 2012; Johnson et al., 2013; Rosenblatt-Velin et al., 2012; Tomita et al., 2012; Zhou et al., 2012) and kidney (Springer et al., 2014) function in laboratory mice. Conventional echocardiographic measurements, including chamber dimensions, wall thickness, and ejection fraction are routinely obtained to assess cardiac function in mice. Recently, myocardial strain and strain rate measurements (Derumeaux et al., 2008) have been added to functional assessments to provide additional details on regional abnormalities that are not evident using conventional measurements. To date, all studies of strain and strain rate in mice or rats have involved adult animals. Myocardial ultrasound imaging in mice is technically feasible and has potential application in studying the pathophysiology of various cardiovascular and kidney disease.

The main limitations of this technique are its user dependency and the loss of accuracy for scanning some anatomical sites due to poor penetration through air and bones.

2.7. Intravital microscopy

2.7.1. Technique

Intravital microscopy (IVM) is an optical imaging technique that enables live animal imaging at high spatial and temporal resolution. Most commonly it utilizes the visible spectrum plus ultra-violet and near-infrared wavelengths (~300–1100 nm). IVM commonly requires a surgical procedure to access the tissue/organ of interest for microscopy, in which case the animal has to be sacrificed immediately after image acquisition. Most tissues are amenable to this approach including, for example, intestinal mesentery, lung, pancreas and skeletal muscles. Implantation of a dorsal skin fold 'window' chamber provides the ability to image the same tissue *in vivo* repeatedly over days to weeks (Intaglietta and Tompkins, 1973; Padhani et al., 2009; Papenfuss et al., 1979). Here, a metal, plastic or carbon fibre chamber incorporating a glass 'window' holds a skin flap away from the mouse body to enable placement under a microscope objective for transmitted light microscopy (Fig. 5).

Dermal layers from one or both sides of the flap are surgically removed for optical clarity, exposing a striated muscle layer (panniculus carnosus) in the window. This technique also enables implantation of tumour or other tissue/cells onto or into the exposed muscle, resulting in tissue thicknesses of ~100–300 μm. For instance, adipose tissue-derived microvascular fragments, seeded onto porous polyurethane scaffolds, were implanted into dorsal skin fold window chambers in mice to study the effects of ageing on their vascularization (Laschke et al., 2014). For reflected light microscopy *e.g.* epi-fluorescence, other types of 'window' can be surgically implanted for exposing the underlying tissue (Alieva et al., 2014). These include the cranial chamber (Monsky et al., 2002), mammary gland chamber (Shah et al., 2011), lung observation chamber (Hatakawa et al., 2002) and 'body wall' chamber (Tsuzuki et al., 2001).

2.7.2. Vascular and cancer microcirculation applications

Most commonly, IVM is used to investigate vascular morphology and function, stromal or parenchymal cell interactions with blood vessels and gene expression using conventional wide-field light microscopy, with either trans- or epi-illumination. Blood vessels provide the greatest endogenous optical contrast amongst the components of soft tissue enabling measurement of vessel length, diameter and branching patterns without the need for exogenous fluorescent contrast agents (Fig. 5). Red blood cell velocity can also be measured, usually with the aid of fluorescently labeled red blood cells or plasma. Methods involve the use of algorithms that either track individual red cells (Reyes-Aldasoro et al., 2008a) or measure the time difference between matched optical signals received at different locations along flowing vessels (Fontanella et al., 2013). Vascular permeability estimations made from measuring the clearance kinetics of an intravenously administered fluorescent contrast agent such as dextran are also valuable for monitoring vascular integrity (Reyes-Aldasoro et al., 2008b). Microcirculatory abnormalities in cancer, an age-related condition, have been extensively studied using IVM (Lunt et al., 2010), for a review. The tumour vasculature is a sought after therapeutic target and IVM has played a major part in progressing an understanding of the processes involved in tumour vascularization and oxygenation (Brizel et al., 1993; Gaustad et al., 2013; Kimura et al., 1996; Sorg et al., 2005), metastasis (Beerling et al., 2011; Condeelis and Segall, 2003) and response of tumour blood vessels to vascular targeted therapy (Akerman et al., 2013; Strieth et al., 2006; Vajkoczy et al.,

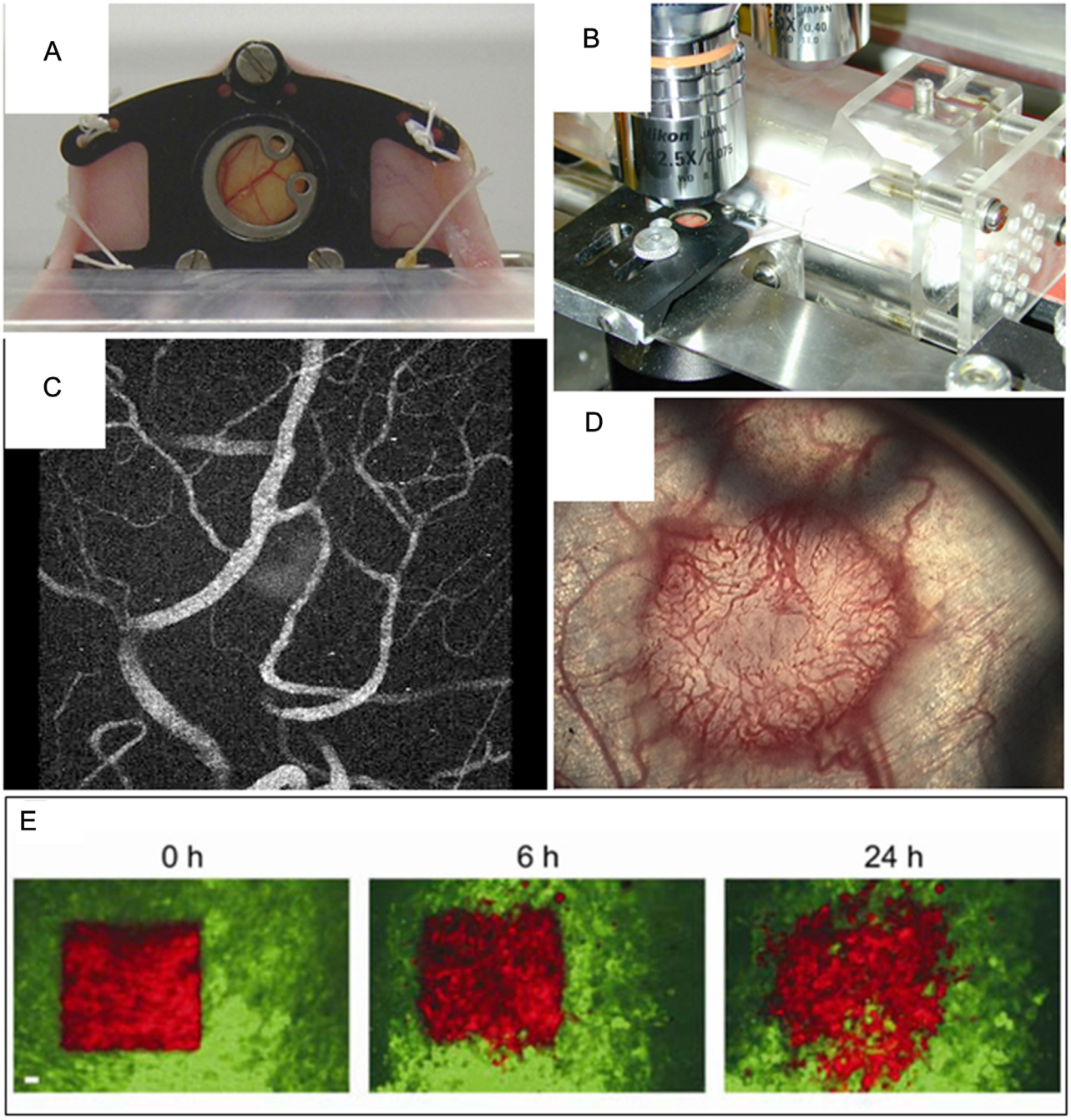

Fig. 5. Intravital microscopy. A) an implanted dorsal skin-fold window chamber in a mouse; B) a mouse bearing a dorsal skin-fold window chamber is restrained in a perspex jig for microscopy; the chamber is immobilised beneath the microscope objective; C) tumour vasculature visualised by intravenous administration of a fluorescent contrast agent and multiphoton fluorescence microscopy; D) low power brightfield view of a tumour growing in a window chamber; the eyelets of the circlip that keeps the glass coverslip overlying the tumour in place can be seen out-of-focus E): tumour cells were labelled with Dendra2, a photo-switchable fluorophore; non-photoswitched are green and photo-switched are red; sequential imaging was used to track the movement of the marked cells. Panel E reprinted by permission from Macmillan Publishers Ltd: Nature Methods, Kedrin et al., 5 (12): 1019–1021, copyright 2008, (Kedrin et al., 2008). (For interpretation of the references to color in this figure legend, the reader is referred to the web version of this article.)

1999), for example. Other ageing pathologies are strongly associated with microvascular defects and have been studied using IVM in mice, for example in cerebral blood flow responses to neuronal activation (Balbi et al., 2015), vasodilatory and microvascular density responses to insulin, exercise and vascular endothelial growth factor in skeletal muscle (Wagenmakers et al., 2015) and microcirculatory response to ischaemia in skin (Harder et al., 2010).

2.7.3. Advances and other applications

Technical advances in microscopy, cameras, fluorophores, computation and image analysis methodology have meant that applications for IVM, which has been a research tool in its basic form for nearly a century, are continually expanding. Microscopes need to be adapted for live animal research to incorporate facilities for animal restraint or anaesthesia and objective lenses with sufficient working distances, magnifications and numerical aper-

tures. Most IVM is performed with cooled CCD (charge-coupled device) cameras and associated hardware that can achieve around 90% quantum efficiency at video rate. Confocal microscopy, often incorporating spinning disc technology or video-rate laser scanning for fast image capture, or multi-photon fluorescence microscopy (Fig. 5) are now commonly used for IVM (Beerling et al., 2011; Brown et al., 2001; Tozer et al., 2005). As well as enabling 3-D imaging, these techniques circumvent the degradation of image quality from light scattered by out-of-focus tissue. This problem can be significant for conventional microscopy even in the thin tissue exposed in window chamber preparations. Multiphoton fluorescence microscopy has the added advantages of increased tissue penetration of the long wavelength light used (from ~40–100 μm for confocal to several hundred μm for multiphoton) and reduced photo-bleaching and photo-toxicity (*i.e.* confined to the focal plane). Multi-photon fluorescence microscopy has been used, for example, to study the effect of ageing on the fate of haematopoietic stem cells in the marrow of long bones (Kohler et al., 2009). Hyperspectral imaging incorporates an optical filtering system in front of the IVM camera, enabling capture of multiple images at different visible light wavelengths, which is particularly useful for measurement of blood haemoglobin oxygen saturation, for example (Shonat et al., 1997; Sorg et al., 2005). Optical coherence tomography (OCT) uses light scatter to generate image contrast and so is distinct from other forms of optical microscopy (Fercher et al., 2003). It can be likened to ultrasound imaging as it measures the intensity and timing of back-scattered light instead of sound. Use of long wavelength light, typically 800–1300 nm enables relatively good depth penetration that can exceed 1 mm. Functional extensions to OCT, primarily Doppler and speckle-variance techniques for monitoring microvascular blood flow (Barton and Stromski, 2005), have extended the utility of OCT in intravital studies.

Use of fluorescent probes is a mainstay for bio-imaging in intravital preparations. Conventional organic dyes such as isothyocyanate (FITC) (excitation and emission maxima at 488 and 520 nm respectively) are prone to photo-bleaching but still widely used for image contrast either alone or conjugated to proteins of interest. Chemically sensitive derivatives of FITC enable investigations of tissue pH for example and the phosphorescence life-times of various porphyrin derivatives are oxygen-sensitive (Helmlinger et al., 1997). Newer synthetic dyes such as Alexa-fluors and certain fluorescent nano-crystals (quantum dots) have improved photostability and emission characteristics. Fluorescent proteins (originally green fluorescent protein, GFP, but now expanded to many different types with superior properties) have been applied widely for IVM, primarily as reporters of gene expression and for cell tracking but also, more recently, for probing molecular interactions *via* FRET (Förster Resonance Energy Transfer) (Condeelis et al., 2000; Conway et al., 2014; Erami et al., 2015). Amongst these proteins are ones that experience reversible or irreversible changes to their emission spectra on exposure to specific wavelengths, which may include changes in both intensity (photo-activated, Fig. 5) and emission wavelength (photo-switchable). Use of these recently developed fluorescent proteins are not fully explored for IVM as yet but there is clear potential for their use in tracking different cell populations over time (Kedrin et al., 2008; Pittet and Weissleder, 2011).

2.7.4. Summary of advantages and limitations

Intravital microscopy enables highly sensitive *in vivo* imaging of tissue structure and function at high spatial resolution (cellular and sub-cellular) and at relatively low cost. There are many suitable fluorescent probes available, with increasingly sophisticated properties, and the technique is amenable to use of gene reporters. Use of near-infrared (NIR) probes reduces the problem of depth penetration. However, there are some fundamental limitations of IVM, which are not overcome by modern techniques, notably the necessity for surgery. In addition, where window chambers are used, abnormally high tissue pressures may be induced. Temperature control, toxicity of contrast agents, photo-toxicity and immune reactions are also important considerations. Quantifying IVM data at high spatial resolution and developing analytical methods for deriving accurate descriptions of biological functions are on-going challenges, especially with the vast amounts of imaging data that are now routinely produced and fundamental difficulties associated with quantifying light emission/absorption. Window chambers have been modified for use with MRI scanners (Gaustad et al., 2008) and simultaneous application of IVM with other imaging modalities such as MRI and PET provides an opportunity to exploit the best of each modality.

2.8. Whole body optical imaging

2.8.1. Technique

Whole body optical imaging is based on the excitation of fluorochromes by means of an external light source (fluorescence) or on the light emitted by chemiluminescent enzymatic reactions within the subject (bioluminescence). In both imaging modes, a CCD camera is used to acquire the light signal, most commonly in a 2D planar image. The camera can be cooled down in order to increase its sensitivity to light and therefore acquire weaker signals (Willmann et al., 2008). Typical fluorochromes used are green fluorescent protein (GFP), red fluorescence protein (RFP), rhodamine, or engineered fluorochromes for particular applications (see Section 2.7). Near-infrared (NIR) fluorescent proteins have allowed significant improvements in tissue penetration for *in vivo* imaging (Hassan and Klaunberg, 2004) and avoidance of artifacts from tissue auto-fluorescence (Kovar et al., 2007).

2.8.2. Cancer research

Whole body optical imaging is a sensitive technique but, due to light scattering, spatial resolution is poor. In mouse models, GFP has been used to measure the *in vivo* growth of many different types of tumours, as well as metastatic spread and the effect of drug treatments on tumour growth (Hoffman, 2001). Moreover, genetically engineered light-emitting reporter genes can be used to study *in vivo* protein expression in cancer models and the effect of pharmacological treatments (Willmann et al., 2008). There is a vast literature about optical fluorescence imaging applications for studying cancer; we report here only a few examples. Chen et al. (2003) used a glucose analogue with NIR fluorescence to localize tumours in mice *via* their high rate of glycolysis compared to surrounding normal tissue. In another application Citrin et al. (2004) labeled endostatin with indocyanine dye (Cy5.5) for detecting tumour vasculature. Pesnel et al. (2012) used a monoclonal antibody labeled with a NIR fluorochrome for detecting leukemic foci in a disseminated murine model.

2.8.3. Other applications

GFPs have been used, amongst other fluorescent proteins, for studying gene expression and protein-protein interactions (van Roessel and Brand, 2002), viral infection (Haan et al., 2001), embryonic development (Lipp and Muller, 2004) and in neuroscience (Cruz-Martin and Portera-Cailliau, 2014). In thrombosis mouse models, NIR fluorochromes conjugated to a thrombin-specific oligopeptide substrate (Jaffer et al., 2002) or conjugated to a peptide ligand derived from the amino terminus of alpha2-antiplasmin (Jaffer et al., 2004) have been used in order to image experimental thrombi. NIR proteins have also been used in musculoskeletal applications. For example, Hansch et al. (2004) showed that anti-F4/80 monoclonal antibodies labeled with Cy5.5 can be used to image antigen-induced rheumatoid arthritis in mice. In addition, a cathepsin-B NIR probe showed potential for diagnosis

of early osteoarthritis (Lai et al., 2004) and a protease-activated NIR probe was used for early monitoring of treatment response to antirheumatic drugs (Wunder et al., 2004). For other applications, Wolf et al. (2014) used redox-sensitive GFP for studying oxidative stress in the skin of mice *in vivo*. Hall et al. (2012) used a dynamic multi-wavelength optical imaging system for visualizing physiologically relevant levels of superoxide in specific brain regions, which can be used to study obesity, diabetes, hypertension and the ageing process itself.

2.8.4. Summary of advantages and limitations

Whole body optical imaging is easy to perform, fast and cost efficient compared to PET or MRI for example.

The main limitation is low depth penetration (a few mm in the case of visible dyes) and light scattering, which severely limits its spatial resolution to the order of 1–10 mm. It is these issues that necessitate the use of intravital microscopy (Section 2.7) for many optical imaging applications. While NIR fluorochromes have improved penetration for *in vivo* applications (up to several centimetres (Kovar et al., 2007)), dense tissues such as bones still represent a problem. While most applications are 2D, 3D systems are now available, providing much better locational information (Zhang et al., 2013). The cost effectiveness of whole body optical imaging makes it easy to combine with other *in vivo* imaging modalities such as micro-CT (Barrefelt et al., 2015; Bernthal et al., 2014; Niska et al., 2012) and preclinical-MRI (Bakalova et al., 2015).

3. Considerations in using *in vivo* imaging for studying ageing with mice models

3.1. Standardization and three Rs (reduction, refinement and replacement) of animals in experimental research

Animal experiments are inherently complex (Denayer et al., 2014). Standardized *in vivo* imaging may present an opportunity to monitor aged mice more effectively. Several sets of stringent guidelines, such as the "Animal Research: reporting of *in vivo* experiments (ARRIVE)" guidelines and the "Guidelines for the welfare and use of animals in cancer research" are useful for making experimental procedures involving animals more robust (Kilkenny et al., 2010; Workman et al., 2010). Using guidance from ARRIVE, the international mouse phenotyping consortium uses both male and female animals in all phenotyping studies to account for sexual dimorphism. With the increasing robustness of *in vivo* imaging, it may become a fundamental add-on to the current procedures for disease phenotyping in addition to procedures that determine the endpoints and effects of interventions, such as body weight (Dennis, 2000; Hawkins et al., 2011; Morton, 2000). So far, it is very difficult to standardize techniques, measurements and laboratory environments across laboratories. Therefore, despite producing good quality data, studies between research groups are often not comparable due to a lack of a consensus regarding standardization (Hrabe de Angelis et al., 2015; Richter et al., 2009; van der Staay et al., 2010). Obviously, this results in increased animal usage and wastes resources when studies produce conflicting results. With aged mice representing such a costly investment for laboratories, it will also become even more important for these studies to be efficient, well planned and maximized in a way that obtains the most possible benefit from each animal. *In vivo* imaging inherently maximizes the use of animals due to its non-terminal nature. Moreover, *in vivo* imaging techniques can be combined with other *in vivo* assessments, which can maximize the usefulness of the mice taking part in these studies. For example, traditional *in vivo* measurements can be used to assess a range of factors, as reported in life methods employed by the IMPC in their International Mouse Phenotyping Resource of Standardised Screens and The European Mouse Phenotyping Resource of Standardised Screens (Mallon et al., 2008), such as behaviour, body composition and frailty (Whitehead et al., 2014).

Maximal use of any available techniques for the reduction, replacement and refinement of animal experiments should be a priority for any researcher working with animals (Festing, 2004; Parker and Browne, 2014). *In vivo* imaging, having the potential for reducing measurement variability by tracking the same animal longitudinally when compared to standard cross-sectional design, can reduce animal numbers. *In vivo* imaging measurements are also capable of refining animal experiments as in some cases they can reduce pain, suffering, distress and lasting harm that may be experienced by the animals using other methods. Additionally, better end point evaluation and health measures will increase the quality of animal experiments, increase animal welfare and hopefully reduce the requirement to repeat experiments.

3.2. Animal considerations in longitudinal in vivo imaging with age

Although the imaging modalities presented in this review offer great potential for longitudinal studies, there are still some challenges in their application to mouse models such as complexity of animal monitoring (preclinical-MRI), radiation exposure from the scan (micro-CT) or from the radioactive markers (preclinical-PET and -SPECT), and invasiveness of the procedure (intravital microscopy). Animal considerations when using longitudinal *in vivo* imaging in preclinical research have been extensively reviewed for young and adult animals (Hildebrandt et al., 2008; Tremoleda et al., 2012). However, little is known about the extent ageing may have as a confounding factor. With age, we observe a decline in major physiological functions, including cognitive (Shoji et al., 2016), cardiovascular (Dai and Rabinovitch, 2009), and respiratory (Lowery et al., 2013), an impaired ability to repair stress-induced damage at the cellular level (Kourtis and Tavernarakis, 2011), an altered metabolic footprint (Houtkooper et al., 2011) and thermoregulation (Van Someren, 2007), and an increased level of sensitivity to stress inducers (Shoji et al., 2016). Therefore, special considerations may apply when using these modalities on aged animals, some of which are reported below.

3.2.1. Animal handling

Regardless of the imaging modality, the stress associated with handling of the animals in laboratory routines, preparation for imaging (*e.g.* restraint, injections, surgeries) and the imaging itself creates physiological and metabolic modifications (Meijer et al., 2005, 2006). These changes can affect experimental outcomes, especially in longitudinal settings (*i.e.* repeated handling) where different measurements are performed on each mouse at each time point (*i.e.* scans with different techniques). The capacity adult mice have to cope with stress induced damage, associated with careful monitoring ensures minimal effect of handling. However, in aged mice, because they present an impaired ability to cope with stress, appropriate controls and validations must be carried out to ensure these changes have minimal effects on the outcome of the experiment.

3.2.2. Anaesthesia

Although required to facilitate immobilisation and image acquisition, anaesthesia is accompanied by a depression in respiration rate, heart rate and cardiac output, and a decrease in core temperature (Caro et al., 2013). These changes result in decreased speed of oxygen delivery to tissues, increasing risk of hypoxia. This risk is aggravated with age, as oxygen delivery to the tissues declines (North and Sinclair, 2012), along with respiratory and cardiac func-

tions, thus affecting recovery. Therefore, extra care must be given to aged animals, in terms of monitoring pre- and post-imaging, especially in longitudinal settings. For instance, using inhalation anaesthesia (such as Isoflurane) mixed with medical grade oxygen will help to reduce the risk of hypoxia related to anaesthesia. It will also allow individual responses to anaesthesia to be efficiently monitored. The animal's temperature should also be kept constant during imaging (*e.g.* with hot air or heating pads). Finally, while adult mice can withstand several hours of anaesthesia without apparent short-term effects (Lu et al., 2015b), anaesthesia time should be decided and tested on aged animals to minimise interferences with the experimental outcomes.

3.2.3. Radiation dose

Whether the exposure is intrinsic, when radiotracers are injected for Micro-PET imaging, or is extrinsic, as it is in micro-CT imaging, radiation exposure is a potential limitation of these methodologies. Irradiation is known to cause DNA damage, which is repaired in a couple of days in adult mice (Grudzenski et al., 2010). When longitudinal studies are planned, a compromise between image quality and radiation dose is often reached. This compromise may be more delicate to establish when studying aged mice, as the tissues ability to repair DNA damage declines with age (Grudzenski et al., 2010). The scanning time as well as the time interval between two imaging sessions should therefore be carefully decided to minimise the radiation related effects.

3.2.4. Animal frailty

The ageing process is accompanied by a frailty state that makes the animal more sensitive to external stimuli such as exposure to handling stress or to radiation. Frailty might be exacerbated in longitudinal settings and it is therefore essential to monitor the wellbeing of the animal throughout the experiment and report any changes. This monitoring can be non-invasive and fast, using a recently published approach that quantifies the frailty index for each animal (Whitehead et al., 2014).

3.2.5. Age of the mouse models

The reviewed literature about applications of *in vivo* imaging modalities for studying ageing and age-related disorders (Table 2) revealed that most of the mice models were used in their adulthood (less than 12 months old), during which all physiological processes are healthy and all markers of ageing (*e.g.* DNA damage, oxidative stress, inflammatory cytokines and cellular senescence) (Lopez-Otin et al., 2013) are absent or minimal. This means that although the current models provide precious information on the diseases onset and progression, they might underestimate ageing as a confounding factor. It is therefore recommended to use aged mice, yet to carefully choose the age window for each project, and take extra care when using very old mice, as they present a high frailty index, and numerous tissue dysfunctions that may be unrelated to the study and interfere with the outcome of the experiment by increasing the variability in the data (Miller and Nadon, 2000).

4. Conclusions

Aged mouse models are a powerful tool that can be used to better understand the ageing process. However, the novelty of these mouse models will also pose new challenges to researchers in various forms including phenotyping and endpoint evaluation. State of the art *in vivo* imaging on aged mice enables well-controlled and accurate longitudinal measurements of tissue and organ phenotypes associated with healthy ageing and age-related diseases. It is also possible to combine different imaging techniques, in order to study dysfunction of multiple tissues or the effect of certain pathologies or treatments on different systems. Combining *in vivo* imaging with other *in vivo* methodologies will also help to maximise the data gained from individual mice.

4.1. Future work and perspectives

It has become clear that the single imaging modalities presented in this review have the potential to be combined with each other and with other standard laboratory techniques, in order to exploit the best features of each modality. The standardization of spatial and temporal measurement from such complex techniques is necessary in order to provide reliable and sharable data. Central facilities that contain all the different imaging techniques and expert researchers with multidisciplinary skills (*e.g.* biology, physics, engineering) to run them and interpret the data obtained are highly desirable. Besides providing novel research findings, these *in vivo* techniques will also help with the reduction of animal usage and refinement of techniques.

A number of challenges remain to be addressed, regarding both the individual techniques and combinations thereof. A lot of work needs to be done on animal handling protocols during scanning *in vivo*, *e.g.* to reduce anaesthesia artifacts, and on the design of optimal instrumented animal holders and chambers that can be used in all systems. In particular, specific standardized procedures should be defined for handling aged mice, showing signs of frailty and dysfunction of multiple tissues. Another point that should be considered is the evaluation of the true non-invasiveness of the imaging modalities. This requires more methodological work, in order to investigate how much each modality affects the measurements being made; for example, the use of contrast agents at high concentrations in MRI, or the use of foreign proteins for molecular imaging studies. A further challenge is related to image analyses and merging of data obtained from multi-modality imaging into a single dataset. Due to unavoidable deformation of soft tissues, standard rigid and affine registrations are probably not sufficient and application of nonlinear registration algorithms becomes fundamental.

Overall, multi-modality *in vivo* imaging in mouse models has the potential of providing biomarkers fundamental to investigate the ageing mechanisms and the effects of dysfunction of multiple tissues and organs and systems.

Conflict of interest

None declared.

Acknowledgements

This article is based upon work from COST Action BM1402:MouseAGE, supported by COST (European Cooperation in Science and Technology). ED and MB would like to acknowledge the UK National Centre for the Replacement, Refinement and Reduction of Animals in Research (NC3Rs). Grant number: NC/K000780/1.

References

Abraham, T.P., Dimaano, V.L., Liang, H.Y., 2007. Role of tissue Doppler and strain echocardiography in current clinical practice. Circulation 116, 2597–2609.

Acton, P.D., Kung, H.F., 2003. Small animal imaging with high resolution single photon emission tomography. Nucl. Med. Biol. 30, 889–895.

Afshar-Oromieh, A., Zechmann, C.M., Malcher, A., Eder, M., Eisenhut, M., Linhart, H.G., Holland-Letz, T., Hadaschik, B.A., Giesel, F.L., Debus, J., 2014. Comparison of PET imaging with a 68Ga-labelled PSMA ligand and 18F-choline-based PET/CT for the diagnosis of recurrent prostate cancer. Eur. J. Nucl. Med. Mol. Imaging 41, 11–20.

Akerman, S., Fisher, M., Daniel, R.A., Lefley, D., Reyes-Aldasoro, C.C., Lunt, S.J., Harris, S., Bjorndahl, M., Williams, L.J., Evans, H., Barber, P.R., Prise, V.E., Vojnovic, B., Kanthou, C., Tozer, G.M., 2013. Influence of soluble or

matrix-bound isoforms of vascular endothelial growth factor-A on tumor response to vascular-targeted strategies. Int. J. Cancer 133, 2563–2576.
Alieva, M., Ritsma, L., Weissleder, R., van Rheenen, J., 2014. Imaging windows for long-term intravital imaging. Intravital 3, e29917.
Alvarez-Fischer, D., Blessmann, G., Trosowski, C., Behe, M., Schurrat, T., Hartmann, A., Behr, T.M., Oertel, W.H., Hoglinger, G.U., Hoffken, H., 2007. Quantitative [(123)I]FP-CIT pinhole SPECT imaging predicts striatal dopamine levels, but not number of nigral neurons in different mouse models of Parkinson's disease. Neuroimage 38, 5–12.
Andringa, G., Drukarch, B., Bol, J.G., de Bruin, K., Sorman, K., Habraken, J.B., Booij, J., 2005. Pinhole SPECT imaging of dopamine transporters correlates with dopamine transporter immunohistochemical analysis in the MPTP mouse model of Parkinson's disease. Neuroimage 26, 1150–1158.
Apostolova, I., Wunder, A., Dirnagl, U., Michel, R., Stemmer, N., Lukas, M., Derlin, T., Gregor-Mamoudou, B., Goldschmidt, J., Brenner, W., Buchert, R., 2012. Brain perfusion SPECT in the mouse: normal pattern according to gender and age. Neuroimage 63, 1807–1817.
Aquaro, G.D., Frijia, F., Positano, V., Menichetti, L., Santarelli, M.F., Ardenkjaer-Larsen, J.H., Wiesinger, F., Lionetti, V., Romano, S.L., Bianchi, G., Neglia, D., Giovannetti, G., Schulte, R.F., Recchia, F.A., Landini, L., Lombardi, M., 2013. 3D CMR mapping of metabolism by hyperpolarized 13C-pyruvate in ischemia-reperfusion. JACC Cardiovasc. Imaging 6, 743–744.
Ardenkjaer-Larsen, J.H., Fridlund, B., Gram, A., Hansson, G., Hansson, L., Lerche, M.H., Servin, R., Thaning, M., Golman, K., 2003. Increase in signal-to-noise ratio of >10,000 times in liquid-state NMR. Proc. Natl. Acad. Sci. U. S. A. 100, 10158–10163.
Artaechevarria, X., Perez-Martin, D., Ceresa, M., de Biurrun, G., Blanco, D., Montuenga, L.M., van Ginneken, B., Ortiz-de-Solorzano, C., Munoz-Barrutia, A., 2009. Airway segmentation and analysis for the study of mouse models of lung disease using micro-CT. Phys. Med. Biol. 54, 7009–7024.
Ayadi, A., Birling, M.C., Bottomley, J., Bussell, J., Fuchs, H., Fray, M., Gailus-Durner, V., Greenaway, S., Houghton, R., Karp, N., Leblanc, S., Lengger, C., Maier, H., Mallon, A.M., Marschall, S., Melvin, D., Morgan, H., Pavlovic, G., Ryder, E., Skarnes, W.C., Selloum, M., Ramirez-Solis, R., Sorg, T., Teboul, L., Vasseur, L., Walling, A., Weaver, T., Wells, S., White, J.K., Bradley, A., Adams, D.J., Steel, K.P., Hrabe de Angelis, M., Brown, S.D., Herault, Y., 2012. Mouse large-scale phenotyping initiatives: overview of the European Mouse Disease Clinic (EUMODIC) and of the Wellcome Trust Sanger Institute Mouse Genetics Project. Mamm. Genome 23, 600–610.
Aziz, K., Berger, K., Claycombe, K., Huang, R., Patel, R., Abela, G.S., 2008. Noninvasive detection and localization of vulnerable plaque and arterial thrombosis with computed tomography angiography/positron emission tomography. Circulation 117, 2061–2070.
Baiker, M., Staring, M., Lowik, C.W., Reiber, J.H., Lelieveldt, B.P., 2011. Automated registration of whole-body follow-up MicroCT data of mice. Med. Image Comput. Comput.-Assist. Interv. 14, 516–523.
Bakalova, R., Nikolova, B., Murayama, S., Atanasova, S., Zhelev, Z., Aoki, I., Kato, M., Tsoneva, I., Saga, T., 2015. Passive and electro-assisted delivery of hydrogel nanoparticles in solid tumors, visualized by optical and magnetic resonance imaging in vivo. Anal. Bioanal. Chem. 408, 905–914.
Balbi, M., Ghosh, M., Longden, T.A., Jativa Vega, M., Gesierich, B., Hellal, F., Lourbopoulos, A., Nelson, M.T., Plesnila, N., 2015. Dysfunction of mouse cerebral arteries during early aging. J. Cereb. Blood Flow Metab. 35, 1445–1453.
Balcerzyk, M., Kontaxakis, G., Delgado, M., Garcia-Garcia, L., Correcher, C., Gonzalez, A.J., Gonzalez, A., Rubio, J.L., Benlloch, J.M., Pozo, M.A., 2009. Initial performance evaluation of a high resolution Albira small animal positron emission tomography scanner with monolithic crystals and depth-of-interaction encoding from a user's perspective. Meas. Sci. Technol. 20, 104011.
Bao, Q., Newport, D., Chen, M., Stout, D.B., Chatziioannou, A.F., 2009. Performance evaluation of the inveon dedicated PET preclinical tomograph based on the NEMA NU-4 standards. J. Nucl. Med. 50, 401–408.
Barrefelt, A., Zhao, Y., Larsson, M.K., Egri, G., Kuiper, R.V., Hamm, J., Saghafian, M., Caidahl, K., Brismar, T.B., Aspelin, P., Heuchel, R., Muhammed, M., Dahne, L., Hassan, M., 2015. Fluorescence labeled microbubbles for multimodal imaging. Biochem. Biophys. Res. Commun. 464, 737–742.
Barton, J., Stromski, S., 2005. Flow measurement without phase information in optical coherence tomography images. Opt. Express 13, 5234–5239.
Beaulieu, C., 2002. The basis of anisotropic water diffusion in the nervous system – a technical review. NMR Biomed. 15, 435–455.
Beckmann, N., Schuler, A., Mueggler, T., Meyer, E.P., Wiederhold, K.H., Staufenbiel, M., Krucker, T., 2003. Age-dependent cerebrovascular abnormalities and blood flow disturbances in APP23 mice modeling Alzheimer's disease. J. Neurosci. 23, 8453–8459.
Beerling, E., Ritsma, L., Vrisekoop, N., Derksen, P.W., van Rheenen, J., 2011. Intravital microscopy: new insights into metastasis of tumors. J. Cell Sci. 124, 299–310.
Benjamin, S., Finch, C., Guerin, J., Nelson, J., Olshansky, S.J., Roth, G., Smith, R., 2006. Handbook of Models for Human Aging. Elsevier.
Bergeron, M., Cadorette, J., Tetrault, M.-A., Beaudoin, J.-F., Leroux, J.-D., Fontaine, R., Lecomte, R., 2014. Imaging performance of labpet apd-based digital pet scanners for pre-clinical research. Phys. Med. Biol. 59, 661.
Bernsen, M.R., Vaissier, P.E.B., Van Holen, R., Booij, J., Beekman, F.J., de Jong, M., 2014. The role of preclinical SPECT in oncological and neurological research in combination with either CT or MRI. Eur. J. Nucl. Med. Mol. Imaging 41, 36–49.
Bernthal, N.M., Taylor, B.N., Meganck, J.A., Wang, Y., Shahbazian, J.H., Niska, J.A., Francis, K.P., Miller, L.S., 2014. Combined in vivo optical and microCT imaging to monitor infection, inflammation, and bone anatomy in an orthopaedic implant infection in mice. J. Visualized Exp., e51612.
Bigalke, B., Phinikaridou, A., Andia, M.E., Cooper, M.S., Schuster, A., Wurster, T., Onthank, D., Munch, G., Blower, P., Gawaz, M., Nagel, E., Botnar, R.M., 2014. PET/CT and MR imaging biomarker of lipid-rich plaques using [64Cu]-labeled scavenger receptor (CD68-Fc). Int. J. Cardiol. 177, 287–291.
Bison, S.M., Haeck, J.C., Bol, K., Koelewijn, S.J., Groen, H.C., Melis, M., Veenland, J.F., Bernsen, M.R., de Jong, M., 2015. Optimization of combined temozolomide and peptide receptor radionuclide therapy (PRRT) in mice after multimodality molecular imaging studies. EJNMMI Res. 5, 62.
Bouxsein, M.L., Boyd, S.K., Christiansen, B.A., Guldberg, R.E., Jepsen, K.J., Muller, R., 2010. Guidelines for assessment of bone microstructure in rodents using micro-computed tomography. J. Bone Miner. Res. 25, 1468–1486.
Bové, J., Prou, D., Perier, C., Przedborski, S., 2005. Toxin-induced models of Parkinson's disease. NeuroRx 2, 484–494.
Brizel, D.M., Klitzman, B., Cook, J.M., Edwards, J., Rosner, G., Dewhirst, M.W., 1993. A comparison of tumor and normal tissue microvascular hematocrits and red cell fluxes in a rat window chamber model. Int. J. Radiat. Oncol. Biol. Phys. 25, 269–276.
Brown, E.B., Campbell, R.B., Tsuzuki, Y., Fukumura, D., Jain, R.K., 2001. Measurement of physiological parameters in tumours *in vivo* using MPLSM. Proc. SPIE 4262, 134–145.
Burke, S.N., Barnes, C.A., 2006. Neural plasticity in the ageing brain. Nat. Rev. Neurosci. 7, 30–40.
Cai, J., Li, F., 2013. Single-photon emission computed tomography tracers for predicting and monitoring cancer therapy. Curr. Pharm. Biotechnol. 14, 693–707.
Campbell, G.M., Tiwari, S., Grundmann, F., Purcz, N., Schem, C., Gluer, C.C., 2014. Three-dimensional image registration improves the long-term precision of in vivo micro-computed tomographic measurements in anabolic and catabolic mouse models. Calcif. Tissue Int. 94, 282–292.
Caro, A.C., Hankenson, F.C., Marx, J.O., 2013. Comparison of thermoregulatory devices used during anesthesia of C57BL/6 mice and correlations between body temperature and physiologic parameters. J. Am. Assoc. Lab. Anim. Sci. 52, 577–583.
Chen, Y., Zheng, G., Zhang, Z.H., Blessington, D., Zhang, M., Li, H., Liu, Q., Zhou, L., Intes, X., Achilefu, S., Chance, B., 2003. Metabolism-enhanced tumor localization by fluorescence imaging: in vivo animal studies. Opt. Lett. 28, 2070–2072.
Cheng, C., Tempel, D., van Haperen, R., van der Baan, A., Grosveld, F., Daemen, M.J., Krams, R., de Crom, R., 2006. Atherosclerotic lesion size and vulnerability are determined by patterns of fluid shear stress. Circulation 113, 2744–2753.
Citrin, D., Lee, A.K., Scott, T., Sproull, M., Menard, C., Tofilon, P.J., Camphausen, K., 2004. In vivo tumor imaging in mice with near-infrared labeled endostatin. Mol. Cancer Ther. 3, 481–488.
Condeelis, J., Segall, J.E., 2003. Intravital imaging of cell movement in tumours. Nat. Rev. Cancer 3, 921–930.
Condeelis, J.S., Wyckoff, J., Segall, J.E., 2000. Imaging of cancer invasion and metastasis using green fluorescent protein. Eur. J. Cancer 36, 1671–1680.
Conway, J.R., Carragher, N.O., Timpson, P., 2014. Developments in preclinical cancer imaging: innovating the discovery of therapeutics. Nat. Rev. Cancer 14, 314–328.
Cowey, S., Szafran, A.A., Kappes, J., Zinn, K.R., Siegal, G.P., Desmond, R.A., Kim, H., Evans, L., Hardy, R.W., 2007. Breast cancer metastasis to bone: evaluation of bioluminescent imaging and microSPECT/CT for detecting bone metastasis in immunodeficient mice. Clin. Exp. Metastasis 24, 389–401.
Craik, F., Salthouse, T., 2000. The Handbook of Ageing and Cognition, second ed. Lawrence Erlbaum, Mahwah, NJ.
Cruz-Martin, A., Portera-Cailliau, C., 2014. In vivo imaging of axonal and dendritic structures in neonatal mouse cortex. Cold Spring Harbor Protoc. 2014, 57–64.
Cullen, P., Baetta, R., Bellosta, S., Bernini, F., Chinetti, G., Cignarella, A., von Eckardstein, A., Exley, A., Goddard, M., Hofker, M., et al., 2003. Rupture of the atherosclerotic plaque does a good animal model exist? Arterioscler. Thromb. Vasc. Biol. 23, 535–542.
Dai, D.F., Rabinovitch, P.S., 2009. Cardiac aging in mice and humans: the role of mitochondrial oxidative stress. Trends Cardiovasc. Med. 19, 213–220.
DeGrado, T.R., Coleman, R.E., Wang, S., Baldwin, S.W., Orr, M.D., Robertson, C.N., Polascik, T.J., Price, D.T., 2000. Synthesis and evaluation of 18F-labeled choline as an oncologic tracer for positron emission tomography: initial findings in prostate cancer. Cancer Res. 61, 110–117.
Denayer, T., Stöhr, T., Van Roy, M., 2014. Animal models in translational medicine: validation and prediction. New Horiz. Transl. Med. 2, 5–11.
Dennis Jr., M.B., 2000. Humane endpoints for genetically engineered animal models. ILAR J. 41, 94–98.
Derumeaux, G., Ichinose, F., Raher, M.J., Morgan, J.G., Coman, T., Lee, C., Cuesta, J.M., Thibault, H., Bloch, K.D., Picard, M.H., Scherrer-Crosbie, M., 2008. Myocardial alterations in senescent mice and effect of exercise training: a strain rate imaging study. Circ.: Cardiovasc. Imaging 1, 227–234.
Dimitriu-Leen, A.C., Scholte, A.J., Jacobson, A.F., 2015. 123I-MIBG SPECT for evaluation of patients with heart failure. J. Nucl. Med. 56 (Suppl. 4), 25S–30S.
Dubeau, S., Ferland, G., Gaudreau, P., Beaumont, E., Lesage, F., 2011. Cerebrovascular hemodynamic correlates of aging in the Lou/c rat: a model of healthy aging. Neuroimage 56, 1892–1901.
Duyn, J.H., 2012. The future of ultra-high field MRI and fMRI for study of the human brain. Neuroimage 62, 1241–1248.

Erami, Z., Herrmann, D., Warren, S.C., Nobis, M., McGhee, E.J., Lucas, M.C., Leung, W., Reischmann, N., Mrowinska, A., Schwarz, J.P., Kadir, S., Conway, J.R., Vennin, C., Karim, S.A., Campbell, A.D., Gallego-Ortega, D., Magenau, A., Murphy, K.J., Ridgway, R.A., Law, A.M., Walters, S.N., Grey, S.T., Croucher, D.R., Zhang, L., Herzog, H., Hardeman, E.C., Gunning, P.W., Ormandy, C.J., Evans, T.R., Strathdee, D., Sansom, O.J., Morton, J.P., Anderson, K.I., Timpson, P., 2015. Intravital FRAP imaging using an E-cadherin-GFP mouse reveals disease- and drug-dependent dynamic regulation of cell-cell junctions in live tissue. Cell Rep.

España, S., Marcinkowski, R., Keereman, V., Vandenberghe, S., Van Holen, R., 2014. DigiPET: sub-millimeter spatial resolution small-animal PET imaging using thin monolithic scintillators. Phys. Med. Biol. 59, 3405.

Fercher, A.F., Drexler, C.K., Hitzenberger, C.K., Lasser, T., 2003. Optical coherence tomography – principles and applications. Rep. Prog. Phys. 66, 239–303.

Fernandez-Dominguez, I., Echevarria-Uraga, J.J., Gomez, N., Luka, Z., Wagner, C., Lu, S.C., Mato, J.M., Martinez-Chantar, M.L., Rodriguez-Cuesta, J., 2011. High-frequency ultrasound imaging for longitudinal evaluation of non-alcoholic fatty liver disease progression in mice. Ultrasound Med. Biol. 37, 1161–1169.

Ferruzzi, J., Bersi, M.R., Humphrey, J.D., 2013. Biomechanical phenotyping of central arteries in health and disease: advantages of and methods for murine models. Ann. Biomed. Eng. 41, 1311–1330.

Festing, M.F., 2004. Refinement and reduction through the control of variation. Altern. Lab. Anim. 32 (Suppl. 1A), 259–263.

Firbank, M.J., Wiseman, R.M., Burton, E.J., Saxby, B.K., O'Brien, J.T., Ford, G.A., 2007. Brain atrophy and white matter hyperintensity change in older adults and relationship to blood pressure. Brain atrophy, WMH change and blood pressure. J. Neurol. 254, 713–721.

Fleming, S.M., Fernagut, P.-O., Chesselet, M.-F.c., 2005. Genetic mouse models of parkinsonism: strengths and limitations. NeuroRx 2, 495–503.

Fodero-Tavoletti, M.T., Okamura, N., Furumoto, S., Mulligan, R.S., Connor, A.R., McLean, C.A., Cao, D., Rigopoulos, A., Cartwright, G.A., O'Keefe, G., et al., 2011. 18F-THK523: a novel in vivo tau imaging ligand for Alzheimer's disease. Brain 134, 1089–1100.

Fontanella, A.N., Schroeder, T., Hochman, D.W., Chen, R.E., Hanna, G., Haglund, M.M., Secomb, T.W., Palmer, G.M., Dewhirst, M.W., 2013. Quantitative mapping of hemodynamics in the lung, brain, and dorsal window chamber-grown tumors using a novel, automated algorithm. Microcirculation 20, 724–735.

Franc, B.L., Acton, P.D., Mari, C., Hasegawa, B.H., 2008. Small-animal SPECT and SPECT/CT: important tools for preclinical investigation. J. Nucl. Med. 49, 1651–1663.

Friedberg, M.K., Mertens, L., 2013. Echocardiographic assessment of ventricular synchrony in congenital and acquired heart disease in children. Echocardiography 30, 460–471.

Fueger, B.J., Czernin, J., Hildebrandt, I., Tran, C., Halpern, B.S., Stout, D., Phelps, M.E., Weber, W.A., 2006. Impact of animal handling on the results of 18F-FDG PET studies in mice. J. Nucl. Med. 47, 999–1006.

Gambhir, S.S., 2002. Molecular imaging of cancer with positron emission tomography. Nat. Rev. Cancer 2, 683–693.

Gaustad, J.V., Brurberg, K.G., Simonsen, T.G., Mollatt, C.S., Rofstad, E.K., 2008. Tumor vascularity assessed by magnetic resonance imaging and intravital microscopy imaging. Neoplasia 10, 354–362.

Gaustad, J.V., Simonsen, T.G., Roa, A.M., Rofstad, E.K., 2013. Tumors exposed to acute cyclic hypoxia show increased vessel density and delayed blood supply. Microvasc. Res. 85, 10–15.

Gayetskyy, S., Museyko, O., Kasser, J., Hess, A., Schett, G., Engelke, K., 2014. Characterization and quantification of angiogenesis in rheumatoid arthritis in a mouse model using muCT. BMC Musculoskelet. Disord. 15, 298.

Ghaghada, K.B., Badea, C.T., Karumbaiah, L., Fettig, N., Bellamkonda, R.V., Johnson, G.A., Annapragada, A., 2011. Evaluation of tumor microenvironment in an animal model using a nanoparticle contrast agent in computed tomography imaging. Acad. Radiol. 18, 20–30.

Glatt, V., Canalis, E., Stadmeyer, L., Bouxsein, M.L., 2007. Age-related changes in trabecular architecture differ in female and male C57BL/6J mice. J. Bone Miner. Res. 22, 1197–1207.

Grudzenski, S., Raths, A., Conrad, S., Rube, C.E., Lobrich, M., 2010. Inducible response required for repair of low-dose radiation damage in human fibroblasts. Proc. Natl. Acad. Sci. U. S. A. 107, 14205–14210.

Haan, K.M., Aiyar, A., Longnecker, R., 2001. Establishment of latent Epstein-Barr virus infection and stable episomal maintenance in murine B-cell lines. J. Virol. 75, 3016–3020.

Halade, G.V., Williams, P.J., Lindsey, M.L., Fernandes, G., 2011. Fish oil decreases inflammation and reduces cardiac remodeling in rosiglitazone treated aging mice. Pharmacol. Res. 63, 300–307.

Hall, D.J., Han, S.H., Chepetan, A., Inui, E.G., Rogers, M., Dugan, L.L., 2012. Dynamic optical imaging of metabolic and NADPH oxidase-derived superoxide in live mouse brain using fluorescence lifetime unmixing. J. Cereb. Blood Flow Metab. 32, 23–32.

Hansch, A., Frey, O., Hilger, I., Sauner, D., Haas, M., Schmidt, D., Kurrat, C., Gajda, M., Malich, A., Brauer, R., Kaiser, W.A., 2004. Diagnosis of arthritis using near-infrared fluorochrome Cy5.5. Invest. Radiol. 39, 626–632.

Harder, Y., Amon, M., Wettstein, R., Rucker, M., Schramm, R., Menger, M.D., 2010. Gender-specific ischemic tissue tolerance in critically perfused skin. Langenbecks Arch. Surg. 395, 33–40.

Hartley, C.J., Reddy, A.K., Madala, S., Michael, L.H., Entman, M.L., Taffet, G.E., 2007. Effects of isoflurane on coronary blood flow velocity in young, old and ApoE(-/-) mice measured by Doppler ultrasound. Ultrasound Med. Biol. 33, 512–521.

Hartwig, H., Silvestre-Roig, C., Hendrikse, J., Beckers, L., Paulin, N., Van der Heiden, K., Braster, Q., Drechsler, M., Daemen, M.J., Lutgens, E., Soehnlein, O., 2015. Atherosclerotic plaque destabilization in mice: a comparative study. PLoS One 10, e0141019.

Hassan, M., Klaunberg, B.A., 2004. Biomedical applications of fluorescence imaging in vivo. Comp. Med. 54, 635–644.

Hatakawa, H., Funakoshi, N., Onizuka, M., Yanagi, K., Ohshima, N., Satoh, Y., Yamamoto, T., Ishikawa, S., 2002. Blood flow does not correlate with the size of metastasis in our new intravital observation model of Lewis lung cancer. Microvasc. Res. 64, 32–37.

Hawkins, P., Morton, D.B., Burman, O., Dennison, N., Honess, P., Jennings, M., Lane, S., Middleton, V., Roughan, J.V., Wells, S., Westwood, K., 2011. A guide to defining and implementing protocols for the welfare assessment of laboratory animals: eleventh report of the BVAAWF/FRAME/RSPCA/UFAW Joint Working Group on Refinement. Lab Anim. 45, 1–13.

Hayasaka, N., Nagai, N., Kawao, N., Niwa, A., Yoshioka, Y., Mori, Y., Shigeta, H., Kashiwagi, N., Miyazawa, M., Satou, T., Higashino, H., Matsuo, O., Murakami, T., 2012. In vivo diagnostic imaging using micro-CT: sequential and comparative evaluation of rodent models for hepatic/brain ischemia and stroke. PLoS One 7, e32342.

He, Y.X., Zhang, G., Pan, X.H., Liu, Z., Zheng, L.Z., Chan, C.W., Lee, K.M., Cao, Y.P., Li, G., Wei, L., Hung, L.K., Leung, K.S., Qin, L., 2011. Impaired bone healing pattern in mice with ovariectomy-induced osteoporosis: a drill-hole defect model. Bone 48, 1388–1400.

Heinzel, A., Mohammadkhani Shali, S., Dafotakis, M., Verburg, F.A., Mottaghy, F.M., Winz, O.H., 2015. Comparison of automatic versus manual procedures for the quantification of dopamine D2 receptor availability using I-123-IBZM-SPECT. Nucl. Med. Commun. 36, 1120–1126.

Heiss, W.D., 2014. Radionuclide imaging in ischemic stroke. J. Nucl. Med. 55, 1831–1841.

Helmlinger, G., Yuan, F., Dellian, M., Jain, R.K., 1997. Interstitial pH and pO_2 gradients in solid tumors *in vivo*: high-resolution measurements reveal a lack of correlation. Nat. Med. 3, 177–182.

Henriksen, O.M., Jensen, L.T., Krabbe, K., Guldberg, P., Teerlink, T., Rostrup, E., 2014. Resting brain perfusion and selected vascular risk factors in healthy elderly subjects. PLoS One 9, e97363.

Hildebrandt, I.J., Su, H., Weber, W.A., 2008. Anesthesia and other considerations for in vivo imaging of small animals. ILAR J. 49, 17–26.

Hoffman, R.M., 2001. Visualization of GFP-expressing tumors and metastasis in vivo. Biotechniques 30, 1016-1022–1024-1016.

Hoit, B.D., 2004. Murine physiology: measuring the phenotype. J. Mol. Cell. Cardiol. 37, 377–387.

Houtkooper, R.H., Argmann, C., Houten, S.M., Canto, C., Jeninga, E.H., Andreux, P.A., Thomas, C., Doenlen, R., Schoonjans, K., Auwerx, J., 2011. The metabolic footprint of aging in mice. Sci. Rep. 1, 134.

Hrabe de Angelis, M., Nicholson, G., Selloum, M., White, J.K., Morgan, H., Ramirez-Solis, R., Sorg, T., Wells, S., Fuchs, H., Fray, M., Adams, D.J., Adams, N.C., Adler, T., Aguilar-Pimentel, A., Ali-Hadji, D., Amann, G., Andre, P., Atkins, S., Auburtin, A., Ayadi, A., Becker, J., Becker, L., Bedu, E., Bekeredjian, R., Birling, M.C., Blake, A., Bottomley, J., Bowl, M.R., Brault, V., Busch, D.H., Bussell, J.N., Calzada-Wack, J., Cater, H., Champy, M.F., Charles, P., Chevalier, C., Chiani, F., Codner, G.F., Combe, R., Cox, R., Dalloneau, E., Dierich, A., Di Fenza, A., Doe, B., Duchon, A., Eickelberg, O., Esapa, C.T., Fertak, L.E., Feigel, T., Emelyanova, I., Estabel, J., Favor, J., Flenniken, A., Gambadoro, A., Garrett, L., Gates, H., Gerdin, A.K., Gkoutos, G., Greenaway, S., Glasl, L., Goetz, P., Da Cruz, I.G., Gotz, A., Graw, J., Guimond, A., Hans, W., Hicks, G., Holter, S.M., Hofler, H., Hancock, J.M., Hoehndorf, R., Hough, T., Houghton, R., Hurt, A., Ivandic, B., Jacobs, H., Jacquot, S., Jones, N., Karp, N.A., Katus, H.A., Kitchen, S., Klein-Rodewald, T., Klingenspor, M., Klopstock, T., Lalanne, V., Leblanc, S., Lengger, C., le Marchand, E., Ludwig, T., Lux, A., McKerlie, C., Maier, H., Mandel, J.L., Marschall, S., Mark, M., Melvin, D.G., Meziane, H., Micklich, K., Mittelhauser, C., Monassier, L., Moulaert, D., Muller, S., Naton, B., Neff, F., Nolan, P.M., Nutter, L.M., Ollert, M., Pavlovic, G., Pellegata, N.S., Peter, E., Petit-Demouliere, B., Pickard, A., Podrini, C., Potter, P., Pouilly, L., Puk, O., Richardson, D., Rousseau, S., Quintanilla-Fend, L., Quwailid, M.M., Racz, I., Rathkolb, B., Riet, F., Rossant, J., Roux, M., Rozman, J., Ryder, E., Salisbury, J., Santos, L., Schable, K.H., Schiller, E., Schrewe, A., Schulz, H., Steinkamp, R., Simon, M., Stewart, M., Stoger, C., Stoger, T., Sun, M., Sunter, D., Teboul, L., Tilly, I., Tocchini-Valentini, G.P., Tost, M., Treise, I., Vasseur, L., Velot, E., Vogt-Weisenhorn, D., Wagner, C., Walling, A., Wattenhofer-Donze, M., Weber, B., Wendling, O., Westerberg, H., Willershauser, M., Wolf, E., Wolter, A., Wood, J., Wurst, W., Yildirim, A.O., Zeh, R., Zimmer, A., Zimprich, A., Holmes, C., Steel, K.P., Herault, Y., Gailus-Durner, V., Mallon, A.M., Brown, S.D., et al., 2015. Analysis of mammalian gene function through broad-based phenotypic screens across a consortium of mouse clinics. Nat. Genet. 47, 969–978.

Hwang, J.J., Liao, M.H., Yen, T.C., Wey, S.P., Lin, K.J., Pan, W.H., Chen, J.C., Ting, G., 2002. Biodistribution study of [99mTc] TRODAT-1 alone or combined with other dopaminergic drugs in mice with macroautoradiography. Appl. Radiat. Isot. 57, 35–42.

Ikonomovic, M.D., Klunk, W.E., Abrahamson, E.E., Mathis, C.A., Price, J.C., Tsopelas, N.D., Lopresti, B.J., Ziolko, S., Bi, W., Paljug, W.R., et al., 2008. Post-mortem correlates of in vivo PiB-PET amyloid imaging in a typical case of Alzheimer's disease. Brain 131, 1630–1645.

Intaglietta, M., Tompkins, W.R., 1973. Microvascular measurements by video image shearing and splitting. Microvasc. Res. 5, 309–312.

Ittmann, M., Huang, J., Radaelli, E., Martin, P., Signoretti, S., Sullivan, R., Simons, B.W., Ward, J.M., Robinson, B.D., Chu, G.C., 2013. Animal models of human prostate cancer: the consensus report of the New York meeting of the Mouse Models of Human Cancers Consortium Prostate Pathology Committee. Cancer Res. 73, 2718–2736.

Jack, C.R., Wiste, H.J., Vemuri, P., Weigand, S.D., Senjem, M.L., Zeng, G., Bernstein, M.A., Gunter, J.L., Pankratz, V.S., Aisen, P.S., et al., 2010. Brain beta-amyloid measures and magnetic resonance imaging atrophy both predict time-to-progression from mild cognitive impairment to Alzheimer's disease. Brain 133, 3336–3348.

Jackson, M.F., Luong, D., Vang, D.D., Garikipati, D.K., Stanton, J.B., Nelson, O.L., Rodgers, B.D., 2012. The aging myostatin null phenotype: reduced adiposity, cardiac hypertrophy, enhanced cardiac stress response, and sexual dimorphism. J. Endocrinol. 213, 263–275.

Jaffer, F.A., Tung, C.H., Gerszten, R.E., Weissleder, R., 2002. In vivo imaging of thrombin activity in experimental thrombi with thrombin-sensitive near-infrared molecular probe. Arterioscler. Thromb. Vasc. Biol. 22, 1929–1935.

Jaffer, F.A., Tung, C.H., Wykrzykowska, J.J., Ho, N.H., Houng, A.K., Reed, G.L., Weissleder, R., 2004. Molecular imaging of factor XIIIa activity in thrombosis using a novel, near-infrared fluorescent contrast agent that covalently links to thrombi. Circulation 110, 170–176.

Johnson, T.L., Tulis, D.A., Keeler, B.E., Virag, J.A., Lust, R.M., Clemens, S., 2013. The dopamine D3 receptor knockout mouse mimics aging-related changes in autonomic function and cardiac fibrosis. PLoS One 8, e74116.

Johnson, K.A., 2007. Imaging techniques for small animal imaging models of pulmonary disease: micro-CT. Toxicol. Pathol. 35, 59–64.

Justice, M.J., Siracusa, L.D., Stewart, A.F., 2011. Technical approaches for mouse models of human disease. Dis. Models Mech. 4, 305–310.

Kapourchali, F.R., Gangadaran Surendiran, L.C., Uitz, E., Bahadori, B., Moghadasian, M.H., 2014. Animal models of atherosclerosis. World J. Clin. Cases: WJCC 2, 126.

Kedrin, D., Gligorijevic, B., Wyckoff, J., Verkhusha, V.V., Condeelis, J., Segall, J.E., van Rheenen, J., 2008. Intravital imaging of metastatic behavior through a mammary imaging window. Nat. Methods 5, 1019–1021.

Kennerley, A.J., Mayhew, J.E., Boorman, L., Zheng, Y., Berwick, J., 2012. Is optical imaging spectroscopy a viable measurement technique for the investigation of the negative BOLD phenomenon? A concurrent optical imaging spectroscopy and fMRI study at high field (7 T). Neuroimage 61, 10–20.

Kepez, A., Akdogan, A., Sade, L.E., Deniz, A., Kalyoncu, U., Karadag, O., Hayran, M., Aytemir, K., Ertenli, I., Kiraz, S., Calguneri, M., Kabakci, G., Tokgozoglu, L., 2008. Detection of subclinical cardiac involvement in systemic sclerosis by echocardiographic strain imaging. Echocardiography 25, 191–197.

Kilkenny, C., Browne, W.J., Cuthill, I.C., Emerson, M., Altman, D.G., 2010. Improving bioscience research reporting: the ARRIVE guidelines for reporting animal research. PLoS Biol. 8, e1000412.

Kimura, K., Braun, R.D., Ong, E.T., Hsu, R., Secomb, T.W., Papahadjopoulos, D., Hong, K., Dewhirst, M.W., 1996. Fluctuations in red cell flux in tumor microvessels can lead to transient hypoxia and reoxygenation in tumor parenchyma. Cancer Res. 56, 5522–5528.

Klinck, J., Boyd, S.K., 2008. The magnitude and rate of bone loss in ovariectomized mice differs among inbred strains as determined by longitudinal in vivo micro-computed tomography. Calcif. Tissue Int. 83, 70–79.

Klunk, W.E., Engler, H., Nordberg, A., Wang, Y., Blomqvist, G., Holt, D.P., Bergström, M., Savitcheva, I., Huang, G.-F., Estrada, S., 2004. Imaging brain amyloid in Alzheimer's disease with Pittsburgh Compound-B. Ann. Neurol. 55, 306–319.

Kohler, A., Schmithorst, V., Filippi, M.D., Ryan, M.A., Daria, D., Gunzer, M., Geiger, H., 2009. Altered cellular dynamics and endosteal location of aged early hematopoietic progenitor cells revealed by time-lapse intravital imaging in long bones. Blood 114, 290–298.

Kourtis, N., Tavernarakis, N., 2011. Cellular stress response pathways and ageing: intricate molecular relationships. EMBO J. 30, 2520–2531.

Kovar, J.L., Simpson, M.A., Schutz-Geschwender, A., Olive, D.M., 2007. A systematic approach to the development of fluorescent contrast agents for optical imaging of mouse cancer models. Anal. Biochem. 367, 1–12.

Kratochwil, C., Giesel, F.L., Eder, M., Afshar-Oromieh, A., Bene\vsová, M., Mier, W., Kopka, K., Haberkorn, U., 2015. [177Lu] Lutetium-labelled PSMA ligand-induced remission in a patient with metastatic prostate cancer. Eur. J. Nucl. Med. Mol. Imaging 42, 987–988.

Kwong, K.K., Belliveau, J.W., Chesler, D.A., Goldberg, I.E., Weisskoff, R.M., Poncelet, B.P., Kennedy, D.N., Hoppel, B.E., Cohen, M.S., Turner, R., et al., 1992. Dynamic magnetic resonance imaging of human brain activity during primary sensory stimulation. Proc. Natl. Acad. Sci. U. S. A. 89, 5675–5679.

Lai, W.F., Chang, C.H., Tang, Y., Bronson, R., Tung, C.H., 2004. Early diagnosis of osteoarthritis using cathepsin B sensitive near-infrared fluorescent probes. Osteoarthritis Cartilage 12, 239–244.

Laitinen, I., Saraste, A., Weidl, E., Poethko, T., Weber, A.W., Nekolla, S.G., Leppanen, P., Yla-Herttuala, S., Holzlwimmer, G., Walch, A., Esposito, I., Wester, H.J., Knuuti, J., Schwaiger, M., 2009. Evaluation of alphavbeta3 integrin-targeted positron emission tomography tracer 18F-galacto-RGD for imaging of vascular inflammation in atherosclerotic mice. Circ.: Cardiovasc. Imaging 2, 331–338.

Lalwani, K., Giddabasappa, A., Li, D., Olson, P., Simmons, B., Shojaei, F., Van Arsdale, T., Christensen, J., Jackson-Fisher, A., Wong, A., Lappin, P.B., Eswaraka, J., 2013. Contrast agents for quantitative microCT of lung tumors in mice. Comp. Med. 63, 482–490.

Lambers, F.M., Kuhn, G., Schulte, F.A., Koch, K., Muller, R., 2012. Longitudinal assessment of in vivo bone dynamics in a mouse tail model of postmenopausal osteoporosis. Calcif. Tissue Int. 90, 108–119.

Lambers, F.M., Kuhn, G., Weigt, C., Koch, K.M., Schulte, F.A., Muller, R., 2015. Bone adaptation to cyclic loading in murine caudal vertebrae is maintained with age and directly correlated to the local micromechanical environment. J. Biomech. 48, 1873–2380.

Laperre, K., Depypere, M., van Gastel, N., Torrekens, S., Moermans, K., Bogaerts, R., Maes, F., Carmeliet, G., 2011. Development of micro-CT protocols for in vivo follow-up of mouse bone architecture without major radiation side effects. Bone 49, 613–622.

Laschke, M.W., Grasser, C., Kleer, S., Scheuer, C., Eglin, D., Alini, M., Menger, M.D., 2014. Adipose tissue-derived microvascular fragments from aged donors exhibit an impaired vascularisation capacity. Eur. Cell Mater. 28, 287–298.

Lee, H.Y., Jeong, K.H., Choi, C.S., 2014. In-depth metabolic phenotyping of genetically engineered mouse models in obesity and diabetes. Mamm. Genome 25, 508–521.

Levchuk, A., Zwahlen, A., Weigt, C., Lambers, F.M., Badilatti, S.D., Schulte, F.A., Kuhn, G., Muller, R., 2014. The Clinical Biomechanics Award 2012 – presented by the European Society of Biomechanics: large scale simulations of trabecular bone adaptation to loading and treatment. Clin. Biomech. (Bristol, Avon) 29, 355–362.

Li, D., Shimamura, T., Ji, H., Chen, L., Haringsma, H.J., McNamara, K., Liang, M.-C., Perera, S.A., Zaghlul, S., Borgman, C.L., 2007. Bronchial and peripheral murine lung carcinomas induced by T790M-L858R mutant EGFR respond to HKI-272 and rapamycin combination therapy. Cancer Cell 12, 81–93.

Li, M., Jirapatnakul, A., Biancardi, A., Riccio, M.L., Weiss, R.S., Reeves, A.P., 2013. Growth pattern analysis of murine lung neoplasms by advanced semi-automated quantification of micro-CT images. PLoS One 8, e83806.

Lienemann, P.S., Metzger, S., Kivelio, A.S., Blanc, A., Papageorgiou, P., Astolfo, A., Pinzer, B.R., Cinelli, P., Weber, F.E., Schibli, R., Behe, M., Ehrbar, M., 2015. Longitudinal in vivo evaluation of bone regeneration by combined measurement of multi-pinhole SPECT and micro-CT for tissue engineering. Sci. Rep. 5, 10238.

Lin, A.J., Liu, G., Castello, N.A., Yeh, J.J., Rahimian, R., Lee, G., Tsay, V., Durkin, A.J., Choi, B., LaFerla, F.M., Chen, Z., Green, K.N., Tromberg, B.J., 2014. Optical imaging in an Alzheimer's mouse model reveals amyloid-beta-dependent vascular impairment. Neurophotonics 1, 011005.

Lipp, M., Muller, G., 2004. Lymphoid organogenesis: getting the green light from RORgamma(t). Nat. Immunol. 5, 12–14.

Liu, Y.Y., Brandt, M.P., Shen, D.H., Kloos, R.T., Zhang, X., Jhiang, S.M., 2011. Single photon emission computed tomography imaging for temporal dynamics of thyroidal and salivary radionuclide accumulation in 17-allyamino-17-demothoxygeldanamycin-treated thyroid cancer mouse model. Endocr. Relat. Cancer 18, 27–37.

Liu, Y., Pierce, R., Luehmann, H.P., Sharp, T.L., Welch, M.J., 2013. PET imaging of chemokine receptors in vascular injury-accelerated atherosclerosis. J. Nucl. Med. 54, 1135–1141.

Logothetis, N.K., Pauls, J., Augath, M., Trinath, T., Oeltermann, A., 2001. Neurophysiological investigation of the basis of the fMRI signal. Nature 412, 150–157.

Lopez-Otin, C., Blasco, M.A., Partridge, L., Serrano, M., Kroemer, G., 2013. The hallmarks of aging. Cell 153, 1194–1217.

Lowery, E.M., Brubaker, A.L., Kuhlmann, E., Kovacs, E.J., 2013. The aging lung. Clin. Interv. Aging 8, 1489–1496.

Lu, Y., Boudiffa, M., Dall'Ara, E., Bellantuono, I., Viceconti, M., 2015a. Evaluation of in-vivo measurement errors associated with micro-computed tomography scans by means of the bone surface distance approach. Med. Eng. Phys. 37, 1091–1097.

Lu, Y., Boudiffa, M., Dall'Ara, E., Bellantuono, I., Viceconti, M., 2015b. Evaluation of in-vivo measurement errors associated with micro-computed tomography scans by means of the bone surface distance approach. Med. Eng. Phys. 37, 1091–1097.

Lunt, S.J., Gray, C., Reyes-Aldasoro, C.C., Matcher, S.J., Tozer, G.M., 2010. Application of intravital microscopy in studies of tumor microcirculation. J. Biomed. Opt. 15, 011113.

Lusic, H., Grinstaff, M.W., 2013. X-ray-computed tomography contrast agents. Chem. Rev. 113, 1641–1666.

Luu, Y.K., Lublinsky, S., Ozcivici, E., Capilla, E., Pessin, J.E., Rubin, C.T., Judex, S., 2009. In vivo quantification of subcutaneous and visceral adiposity by micro-computed tomography in a small animal model. Med. Eng. Phys. 31, 34–41.

Maheswaran, S., Barjat, H., Rueckert, D., Bate, S.T., Howlett, D.R., Tilling, L., Smart, S.C., Pohlmann, A., Richardson, J.C., Hartkens, T., Hill, D.L., Upton, N., Hajnal, J.V., James, M.F., 2009. Longitudinal regional brain volume changes quantified in normal aging and Alzheimer's APP × PS1 mice using MRI. Brain Res. 1270, 19–32.

Mallon, A.M., Blake, A., Hancock, J.M., 2008. EuroPhenome and EMPReSS: online mouse phenotyping resource. Nucleic Acids Res. 36, D715–D718.

Manook, A., Yousefi, B.H., Willuweit, A., Platzer, S., Reder, S., Voss, A., Huisman, M., Settles, M., Neff, F., Velden, J., et al., 2012. Small-animal PET imaging of amyloid-beta plaques with [11C] PiB and its multi-modal validation in an APP/PS1 mouse model of Alzheimer's disease. PLoS One 7, e31310.

Marenzana, M., Hagen, C.K., Borges, P.D., Endrizzi, M., Szafraniec, M.B., Vincent, T.L., Rigon, L., Arfelli, F., Menk, R.H., Olivo, A., 2014. Synchrotron- and laboratory-based X-ray phase-contrast imaging for imaging mouse articular cartilage in the absence of radiopaque contrast agents. Philos. Transact. A: Math. Phys. Eng. Sci. 372, 20130127.

Matoba, T., Sato, K., Egashira, K., 2013. Mouse models of plaque rupture. Curr. Opin. Lipidol. 24, 419–425.
McGirr, R., Hu, S., Yee, S.-P., Kovacs, M.S., Lee, T.-Y., Dhanvantari, S., 2011. Towards PET imaging of intact pancreatic beta cell mass: a transgenic strategy. Mol. Imaging Biol. 13, 962–972.
Meijer, M.K., Lemmens, A.G., Van Zutphen, B.F., Baumans, V., 2005. Urinary corticosterone levels in mice in response to intraperitoneal injections with saline. J. Appl. Anim. Welf. Sci. 8, 279–283.
Meijer, M.K., Spruijt, B.M., van Zutphen, L.F., Baumans, V., 2006. Effect of restraint and injection methods on heart rate and body temperature in mice. Lab. Anim. 40, 382–391.
Melrose, H.L., Lincoln, S.J., Tyndall, G.M., Farrer, M.J., 2006. Parkinson's disease: a rethink of rodent models. Exp. Brain Res. 173, 196–204.
Memon, A.A., Jakobsen, S., Dagnaes-Hansen, F., Sorensen, B.S., Keiding, S., Nexo, E., 2009. Positron emission tomography (PET) imaging with [11C]-labeled erlotinib: a micro-PET study on mice with lung tumor xenografts. Cancer Res. 69, 873–878.
Meyer, P.T., Salber, D., Schiefer, J., Cremer, M., Schaefer, W.M., Kosinski, C.M., Langen, K.J., 2008. Cerebral kinetics of the dopamine D(2) receptor ligand [(123)I]IBZM in mice. Nucl. Med. Biol. 35, 467–473.
Miller, R.A., Nadon, N.L., 2000. Principles of animal use for gerontological research. J. Gerontol. A Biol. Sci. Med. Sci. 55, B117–B123.
Minoshima, S., Cross, D., 2008. In vivo imaging of axonal transport using MRI: aging and Alzheimer's disease. Eur. J. Nucl. Med. Mol. Imaging 35 (Suppl. 1), S89–S92.
Mitchell, H.H., Hamilton, T.S., Steggerda, F.R., Bean, H.W., 1945. The chemical composition of the adult human body and its bearing on the biochemistry of growth. J. Biol. Chem. 158, 625–637.
Monsky, W.L., Mouta Carreira, C., Tsuzuki, Y., Gohongi, T., Fukumura, D., Jain, R.K., 2002. Role of host microenvironment in angiogenesis and microvascular functions in human breast cancer xenografts: mammary fat pad versus cranial tumors. Clin. Cancer Res. 8, 1008–1013.
Morton, D.B., 2000. A systematic approach for establishing humane endpoints. ILAR J. 41, 80–86.
Mosley, M., Knight, J., Neesse, A., Michl, P., Iezzi, M., Kersemans, V., Cornelissen, B., 2015. Claudin-4 SPECT imaging allows detection of aplastic lesions in a mouse model of breast cancer. J. Nucl. Med. 56, 745–751.
Nagy, K., Tóth, M., Major, P., Patay, G., Egri, G.H.H., Häggkvist, J., Varrone, A., Farde, L., Halldin, C., Gulyás, B., 2013. Performance evaluation of the small-animal nanoScan PET/MRI system. J. Nucl. Med. 54, 1825–1832.
Nahrendorf, M., Zhang, H., Hembrador, S., Panizzi, P., Sosnovik, D.E., Aikawa, E., Libby, P., Swirski, F.K., Weissleder, R., 2008. Nanoparticle PET-CT imaging of macrophages in inflammatory atherosclerosis. Circulation 117, 379–387.
Nebuloni, L., Kuhn, G.A., Vogel, J., Muller, R., 2014. A novel in vivo vascular imaging approach for hierarchical quantification of vasculature using contrast enhanced micro-computed tomography. PLoS One 9, e86562.
Nie, X., Laforest, R., Elvington, A., Randolph, G.J., Zheng, J., Voller, T., Abendschein, D.R., Lapi, S., Woodard, P.K., 2016. PET/MR imaging of hypoxic atherosclerosis using 64Cu-ATSM in a rabbit model. J. Nucl. Med. [Epub ahead of print].
Niccoli, T., Partridge, L., 2012. Ageing as a risk factor for disease. Curr. Biol. 22, R741–R752.
Niska, J.A., Meganck, J.A., Pribaz, J.R., Shahbazian, J.H., Lim, E., Zhang, N., Rice, B.W., Akin, A., Ramos, R.I., Bernthal, N.M., Francis, K.P., Miller, L.S., 2012. Monitoring bacterial burden, inflammation and bone damage longitudinally using optical and muCT imaging in an orthopaedic implant infection in mice. PLoS One 7, e47397.
Nordberg, A., 2004. PET imaging of amyloid in Alzheimer's disease. Lancet Neurol. 3, 519–527.
Norfray, J.F., Provenzale, J.M., 2004. Alzheimer's disease: neuropathologic findings and recent advances in imaging. AJR Am. J. Roentgenol. 182, 3–13.
North, B.J., Sinclair, D.A., 2012. The intersection between aging and cardiovascular disease. Circ. Res. 110, 1097–1108.
Oberg, J., Spenger, C., Wang, F.H., Andersson, A., Westman, E., Skoglund, P., Sunnemark, D., Norinder, U., Klason, T., Wahlund, L.O., Lindberg, M., 2008. Age related changes in brain metabolites observed by 1H MRS in APP/PS1 mice. Neurobiol. Aging 29, 1423–1433.
Ogawa, S., Lee, T.M., Kay, A.R., Tank, D.W., 1990. Brain magnetic resonance imaging with contrast dependent on blood oxygenation. Proc. Natl. Acad. Sci. U. S. A. 87, 9868–9872.
Ohta, S., Lai, E.W., Morris, J.C., Bakan, D.A., Klaunberg, B., Cleary, S., Powers, J.F., Tischler, A.S., Abu-Asab, M., Schimel, D., Pacak, K., 2006. MicroCT for high-resolution imaging of ectopic pheochromocytoma tumors in the liver of nude mice. Int. J. Cancer 119, 2236–2241.
Okamura, N., Furumoto, S., Fodero-Tavoletti, M.T., Mulligan, R.S., Harada, R., Yates, P., Pejoska, S., Kudo, Y., Masters, C.L., Yanai, K., et al., 2014. Non-invasive assessment of Alzheimer's disease neurofibrillary pathology using 18F-THK5105 PET. Brain, awu064.
Owen, D., Lindsay, A., Choudhury, R., Fayad, Z., 2011. Imaging of atherosclerosis. Annu. Rev. Med. 62, 25.
Padhani, A.R., Liu, G., Koh, D.M., Chenevert, T.L., Thoeny, H.C., Takahara, T., Dzik-Jurasz, A., Ross, B.D., Van Cauteren, M., Collins, D., Hammoud, D.A., Rustin, G.J., Taouli, B., Choyke, P.L., 2009. Diffusion-weighted magnetic resonance imaging as a cancer biomarker: consensus and recommendations. Neoplasia 11, 102–125.
Pan, W.J., Thompson, G., Magnuson, M., Majeed, W., Jaeger, D., Keilholz, S., 2010. Simultaneous FMRI and electrophysiology in the rodent brain. J. Visualized Exp. 9, 1901.
Papenfuss, H.D., Gross, J.F., Intaglietta, M., Treese, F.A., 1979. A transparent access chamber for the rat dorsal skin fold. Microvasc. Res. 18, 311–318.
Parker, R.M., Browne, W.J., 2014. The place of experimental design and statistics in the 3Rs. ILAR J. 55, 477–485.
Perilli, E., Cantley, M., Marino, V., Crotti, T.N., Smith, M.D., Haynes, D.R., Dharmapatni, A.A., 2015. Quantifying not only bone loss, but also soft tissue swelling, in a murine inflammatory arthritis model using micro-computed tomography. Scand. J. Immunol. 81, 142–150.
Pesnel, S., Pillon, A., Creancier, L., Lerondel, S., Le Pape, A., Recher, C., Demur, C., Guilbaud, N., Kruczynski, A., 2012. Optical imaging of disseminated leukemia models in mice with near-infrared probe conjugated to a monoclonal antibody. PLoS One 7, e30690.
Pettegrew, J.W., Withers, G., Panchalingam, K., Post, J.F., 1987. 31P nuclear magnetic resonance (NMR) spectroscopy of brain in aging and Alzheimer's disease. J. Neural Transm. Suppl. 24, 261–268.
Phelps, M.E., 2000. Positron emission tomography provides molecular imaging of biological processes. Proc. Natl. Acad. Sci. U. S. A. 97, 9226–9233.
Pierroz, D.D., Bonnet, N., Baldock, P.A., Ominsky, M.S., Stolina, M., Kostenuik, P.J., Ferrari, S.L., 2010. Are osteoclasts needed for the bone anabolic response to parathyroid hormone? A study of intermittent parathyroid hormone with denosumab or alendronate in knock-in mice expressing humanized RANKL. J. Biol. Chem. 285, 28164–28173.
Piscaer, T.M., van Osch, G.J., Verhaar, J.A., Weinans, H., 2008. Imaging of experimental osteoarthritis in small animal models. Biorheology 45, 355–364.
Pissarek, M., Meyer-Kirchrath, J., Hohlfeld, T., Vollmar, S., Oros-Peusquens, A.M., Flogel, U., Jacoby, C., Krugel, U., Schramm, N., 2009. Targeting murine heart and brain: visualisation conditions for multi-pinhole SPECT with (99m)Tc- and (123)I-labelled probes. Eur. J. Nucl. Med. Mol. Imaging 36, 1495–1509.
Pittet, M.J., Weissleder, R., 2011. Intravital imaging. Cell 147, 983–991.
Prince, M., Knapp, M.A., Guerchet, M., McCrone, P., Prina, M., Comas-Herrera, A., Wittenberg, R., Adelaja, B., Hu, B., King, D., Rehill, A., Salimkumar, D., 2014. Dementia UK: Update, second ed. King's College London.
Ram, R., Mickelsen, D.M., Theodoropoulos, C., Blaxall, B.C., 2011. New approaches in small animal echocardiography: imaging the sounds of silence. Am. J. Physiol. Heart Circ. Physiol. 301, H1765–H1780.
Raman, V., Pathak, A.P., Glunde, K., Artemov, D., Bhujwalla, Z.M., 2007. Magnetic resonance imaging and spectroscopy of transgenic models of cancer. NMR Biomed. 20, 186–199.
Ravoori, M., Czaplinska, A.J., Sikes, C., Han, L., Johnson, E.M., Qiao, W., Ng, C., Cody, D.D., Murphy, W.A., Do, K.A., Navone, N.M., Kundra, V., 2010. Quantification of mineralized bone response to prostate cancer by noninvasive in vivo microCT and non-destructive ex vivo microCT and DXA in a mouse model. PLoS One 5, e9854.
Raz, N., Rodrigue, K.M., 2006. Differential aging of the brain: patterns, cognitive correlates and modifiers. Neurosci. Biobehav. Rev. 30, 730–748.
Raz, N., Lindenberger, U., Rodrigue, K.M., Kennedy, K.M., Head, D., Williamson, A., Dahle, C., Gerstorf, D., Acker, J.D., 2005. Regional brain changes in aging healthy adults: general trends, individual differences and modifiers. Cereb. Cortex 15, 1676–1689.
Razi, H., Birkhold, A.I., Zaslansky, P., Weinkamer, R., Duda, G.N., Willie, B.M., Checa, S., 2015. Skeletal maturity leads to a reduction in the strain magnitudes induced within the bone: a murine tibia study. Acta Biomater. 13, 301–310.
Reyes-Aldasoro, C.C., Akerman, S., Tozer, G.M., 2008a. Measuring the velocity of fluorescently labelled red blood cells with a keyhole tracking algorithm. J. Microsc. 229, 162–173.
Reyes-Aldasoro, C.C., Wilson, I., Prise, V.E., Barber, P.R., Ameer-Beg, S.M., Vojnovic, B., Cunningham, V.J., Tozer, G.M., 2008b. Estimation of apparent tumor vascular permeability from multiphoton fluorescence microscopic images of P22 rat sarcomas in vivo. Microcirculation 15, 65–79.
Richter, S.H., Garner, J.P., Wurbel, H., 2009. Environmental standardization: cure or cause of poor reproducibility in animal experiments? Nat. Methods 6, 257–261.
Robertson, D.M., van Amelsvoort, T., Daly, E., Simmons, A., Whitehead, M., Morris, R.G., Murphy, K.C., Murphy, D.G., 2001. Effects of estrogen replacement therapy on human brain aging: an in vivo 1H MRS study. Neurology 57, 2114–2117.
Rodt, T., von Falck, C., Halter, R., Ringe, K., Shin, H.O., Galanski, M., Borlak, J., 2009. In vivo microCT quantification of lung tumor growth in SPC-raf transgenic mice. Front. Biosci. (Landmark Ed.) 14, 1939–1944.
Rosenblatt-Velin, N., Ogay, S., Felley, A., Stanford, W.L., Pedrazzini, T., 2012. Cardiac dysfunction and impaired compensatory response to pressure overload in mice deficient in stem cell antigen-1. FASEB J. 26, 229–239.
Rosenthal, N., Brown, S., 2007. The mouse ascending: perspectives for human-disease models. Nat. Cell Biol. 9, 993–999.
Ross, R., 1993. The pathogenesis of atherosclerosis: a perspective for the 1990.
Rowland, D.J., Cherry, S.R., 2008. Small-animal preclinical nuclear medicine instrumentation and methodology. Semin. Nucl. Med. 38, 209–222.
Rozman, J., Klingenspor, M., Hrabe de Angelis, M., 2014. A review of standardized metabolic phenotyping of animal models. Mamm. Genome 25, 497–507.
Rudd, J.H., Warburton, E., Fryer, T., Jones, H., Clark, J., Antoun, N., Johnström, P., Davenport, A., Kirkpatrick, P., Arch, B.N., 2002. Imaging atherosclerotic plaque inflammation with [18F]-fluorodeoxyglucose positron emission tomography. Circulation 105, 2708–2711.
Rudin, M., 1992. In-vivo Magnetic Resonance Spectroscopy. Springer-Verlag, Berlin.
Salat, D.H., Kaye, J.A., Janowsky, J.S., 1999. Prefrontal gray and white matter volumes in healthy aging and Alzheimer disease. Arch. Neurol. 56, 338–344.

Sandhu, G.S., Solorio, L., Broome, A.M., Salem, N., Kolthammer, J., Shah, T., Flask, C., Duerk, J.L., 2010. Whole animal imaging. Wiley Interdiscip. Rev. Syst. Biol. Med. 2, 398–421.
Saraste, A., Laitinen, I., Weidl, E., Wildgruber, M., Weber, A.W., Nekolla, S.G., Holzlwimmer, G., Esposito, I., Walch, A., Leppanen, P., Lisinen, I., Luppa, P.B., Yla-Herttuala, S., Wester, H.J., Knuuti, J., Schwaiger, M., 2012. Diet intervention reduces uptake of alphavbeta3 integrin-targeted PET tracer 18F-galacto-RGD in mouse atherosclerotic plaques. J. Nucl. Cardiol. 19, 775–784.
Schäfer, M., Bauder-Wüst, U., Leotta, K., Zoller, F., Mier, W., Haberkorn, U., Eisenhut, M., Eder, M., 2012. A dimerized urea-based inhibitor of the prostate-specific membrane antigen for 68Ga-PET imaging of prostate cancer. EJNMMI Res. 2, 23.
Scheltens, P., Blennow, K., Breteler, M.M.B., de Strooper, B., Frisoni, G.B., Salloway, S., Van der Flier, W.M., 2016. Alzheimer's disease. Lancet 388, 505–517.
Schneider, J.E., Stork, L.A., Bell, J.T., ten Hove, M., Isbrandt, D., Clarke, K., Watkins, H., Lygate, C.A., Neubauer, S., 2008. Cardiac structure and function during ageing in energetically compromised Guanidinoacetate N-methyltransferase (GAMT)-knockout mice—a one year longitudinal MRI study. J. Cardiovasc. Magn. Reson. 10, 9.
Schofield, P.N., Vogel, P., Gkoutos, G.V., Sundberg, J.P., 2012. Exploring the elephant: histopathology in high-throughput phenotyping of mutant mice. Dis. Models Mech. 5, 19–25.
Schug, D., Lerche, C., Weissler, B., Gebhardt, P., Goldschmidt, B., Wehner, J., Dueppenbecker, P.M., Salomon, A., Hallen, P., Kiessling, F., Schulz, V., 2015a. Initial PET Performance Evaluation of a Preclinical Insert for PET/MRI with Digital SiPM Technology.
Schug, D., Wehner, J., Dueppenbecker, P.M., Weissler, B., Gebhardt, P., Goldschmidt, B., Salomon, A., Kiessling, F., Schulz, V., 2015b. PET performance and MRI compatibility evaluation of a digital, ToF-capable PET/MRI insert equipped with clinical scintillators. Phys. Med. Biol. 60, 7045.
Schulte, F.A., Lambers, F.M., Kuhn, G., Muller, R., 2011. In vivo micro-computed tomography allows direct three-dimensional quantification of both bone formation and bone resorption parameters using time-lapsed imaging. Bone 48, 433–442.
Seo, J.W., Baek, H., Mahakian, L.M., Kusunose, J., Hamzah, J., Ruoslahti, E., Ferrara, K.W., 2014. (64)Cu-labeled LyP-1-dendrimer for PET-CT imaging of atherosclerotic plaque. Bioconjugate Chem. 25, 231–239.
Shah, D.K., Veith, J., Bernacki, R.J., Balthasar, J.P., 2011. Evaluation of combined bevacizumab and intraperitoneal carboplatin or paclitaxel therapy in a mouse model of ovarian cancer. Cancer Chemother. Pharmacol. 68, 951–958.
Sharma, S.K., Ebadi, M., 2005. Distribution kinetics of 18 F-DOPA in weaver mutant mice. Mol. Brain Res. 139, 23–30.
Shimizu, S., Kanetaka, H., Hirao, K., Fukasawa, R., Namioka, N., Hatanaka, H., Hirose, D., Umahara, T., Sakurai, H., Hanyu, H., 2016. Neuroimaging for diagnosing dementia with Lewy bodies: what is the best neuroimaging technique in discriminating dementia with Lewy bodies from Alzheimer's disease? Geriatr. Gerontol. Int. [Epub ahead of print].
Shoji, H., Takao, K., Hattori, S., Miyakawa, T., 2016. Age-related changes in behavior in C57BL/6J mice from young adulthood to middle age. Mol. Brain 9, 11.
Shonat, R.D., Wachman, E.S., Niu, W., Koretsky, A.P., Farkas, D.L., 1997. Near-simultaneous hemoglobin saturation and oxygen tension maps in mouse brain using an AOTF microscope. Biophys. J. 73, 1223–1231.
Silva, M.J., Brodt, M.D., Lynch, M.A., Stephens, A.L., Wood, D.J., Civitelli, R., 2012. Tibial loading increases osteogenic gene expression and cortical bone volume in mature and middle-aged mice. PLoS One 7, e34980.
Slawson, S.E., Roman, B.B., Williams, D.S., Koretsky, A.P., 1998. Cardiac MRI of the normal and hypertrophied mouse heart. Magn. Reson. Med. 39, 980–987.
Song, S.K., Kim, J.H., Lin, S.J., Brendza, R.P., Holtzman, D.M., 2004. Diffusion tensor imaging detects age-dependent white matter changes in a transgenic mouse model with amyloid deposition. Neurobiol. Dis. 15, 640–647.
Sorg, B.S., Moeller, B.J., Donovan, O., Cao, Y., Dewhirst, M.W., 2005. Hyperspectral imaging of hemoglobin saturation in tumor microvasculature and tumor hypoxia development. J. Biomed. Opt. 10, 44004.
Sorond, F.A., Kiely, D.K., Galica, A., Moscufo, N., Serrador, J.M., Iloputaife, I., Egorova, S., Dell'Oglio, E., Meier, D.S., Newton, E., Milberg, W.P., Guttmann, C.R., Lipsitz, L.A., 2011. Neurovascular coupling is impaired in slow walkers: the MOBILIZE Boston Study. Ann. Neurol. 70, 213–220.
Sowell, E.R., Peterson, B.S., Thompson, P.M., Welcome, S.E., Henkenius, A.L., Toga, A.W., 2003. Mapping cortical change across the human life span. Nat. Neurosci. 6, 309–315.
Spilt, A., Geeraedts, T., de Craen, A.J., Westendorp, R.G., Blauw, G.J., van Buchem, M.A., 2005. Age-related changes in normal-appearing brain tissue and white matter hyperintensities: more of the same or something else? AJNR Am. J. Neuroradiol. 26, 725–729.
Springer, D.A., Allen, M., Hoffman, V., Brinster, L., Starost, M.F., Bryant, M., Eckhaus, M., 2014. Investigation and identification of etiologies involved in the development of acquired hydronephrosis in aged laboratory mice with the use of high-frequency ultrasound imaging. Pathobiol. Aging Age Relat. Dis. 4.
Stadelmann, V.A., Bonnet, N., Pioletti, D.P., 2011. Combined effects of zoledronate and mechanical stimulation on bone adaptation in an axially loaded mouse tibia. Clin. Biomech. (Bristol, Avon) 26, 101–105.
Starosolski, Z., Villamizar, C.A., Rendon, D., Paldino, M.J., Milewicz, D.M., Ghaghada, K.B., Annapragada, A.V., 2015. Ultra high-resolution in vivo computed tomography imaging of mouse cerebrovasculature using a long circulating blood pool contrast agent. Sci. Rep. 5, 10178.
Stodieck, S.K., Greifzu, F., Goetze, B., Schmidt, K.F., Lowel, S., 2014. Brief dark exposure restored ocular dominance plasticity in aging mice and after a cortical stroke. Exp. Gerontol. 60, 1–11.
Strieth, S., Eichhorn, M.E., Sutter, A., Jonczyk, A., Berghaus, A., Dellian, M., 2006. Antiangiogenic combination tumor therapy blocking alpha(v)-integrins and VEGF-receptor-2 increases therapeutic effects in vivo. Int. J. Cancer 119, 423–431.
Strother, S., Casey, M., Hoffman, E., 1990. Measuring PET scanner sensitivity: relating countrates to image signal-to-noise ratios using noise equivalents counts. IEEE Trans. Nucl. Sci. 37, 783–788.
Sugiyama, T., Saxon, L.K., Zaman, G., Moustafa, A., Sunters, A., Price, J.S., Lanyon, L.E., 2008. Mechanical loading enhances the anabolic effects of intermittent parathyroid hormone (1–34) on trabecular and cortical bone in mice. Bone 43, 238–248.
Suman, R., Beard, J., 2011. Global Health and Aging. World Health Organization.
Swirski, F.K., Nahrendorf, M., 2013. Imaging macrophage development and fate in atherosclerosis and myocardial infarction. Immunol. Cell Biol. 91, 297–303.
Tawakol, A., Migrino, R.Q., Bashian, G.G., Bedri, S., Vermylen, D., Cury, R.C., Yates, D., LaMuraglia, G.M., Furie, K., Houser, S., 2006. In vivo 18F-fluorodeoxyglucose positron emission tomography imaging provides a noninvasive measure of carotid plaque inflammation in patients. J. Am. Coll. Cardiol. 48, 1818–1824.
Tomita, H., Hagaman, J., Friedman, M.H., Maeda, N., 2012. Relationship between hemodynamics and atherosclerosis in aortic arches of apolipoprotein E-null mice on 129S6/SvEvTac and C57BL/6J genetic backgrounds. Atherosclerosis 220, 78–85.
Tozer, G.M., Kanthou, C., Baguley, B.C., 2005. Disrupting tumour blood vessels. Nat. Rev. Cancer 5, 423–435.
Tremoleda, J.L., Kerton, A., Gsell, W., 2012. Anaesthesia and physiological monitoring during in vivo imaging of laboratory rodents: considerations on experimental outcomes and animal welfare. EJNMMI Res. 2, 44.
Tsuzuki, Y., Mouta Carreira, C., Bockhorn, M., Xu, L., Jain, R.K., Fukumura, D., 2001. Pancreas microenvironment promotes VEGF expression and tumor growth: novel window models for pancreatic tumor angiogenesis and microcirculation. Lab. Invest. 81, 1439–1451.
Ullrich, M., Bergmann, R., Peitzsch, M., Zenker, E.F., Cartellieri, M., Bachmann, M., Ehrhart-Bornstein, M., Block, N.L., Schally, A.V., Eisenhofer, G., Bornstein, S.R., Pietzsch, J., Ziegler, C.G., 2016. Multimodal somatostatin receptor theranostics using [(64)Cu]Cu-/[(177)Lu]Lu-DOTA-(Tyr(3))octreotate and AN-238 in a mouse pheochromocytoma model. Theranostics 6, 650–665.
Vajkoczy, P., Menger, M.D., Vollmar, B., Schiling, L., Schmiedek, P., Hirth, K.P., Ullrich, A., Fong, T.A.T., 1999. Inhibition of tumor growth angiogenesis and microcirculation by the novel Flk-1 inhibitor SU5416 as assessed by intravital multi-'fluorescence videomicroscopy. Neoplasia 1, 31–41.
Van Audenhaege, K., Van Holen, R., Vandenberghe, S., Vanhove, C., Metzler, S.D., Moore, S.C., 2015. Review of SPECT collimator selection, optimization, and fabrication for clinical and preclinical imaging. Med. Phys. 42, 4796–4813.
van Roessel, P., Brand, A.H., 2002. Imaging into the future: visualizing gene expression and protein interactions with fluorescent proteins. Nat. Cell Biol. 4, E15–E20.
van der Have, F., Ivashchenko, O., Goorden, M.C., Ramakers, R.M., Beekman, F.J., 2016. High-resolution clustered pinhole 131Iodine SPECT imaging in mice. Nucl. Med. Biol. 43, 506–511.
van der Staay, F.J., Arndt, S.S., Nordquist, R.E., 2010. The standardization-generalization dilemma: a way out. Genes Brain Behav. 9, 849–855.
Van Someren, E.J., 2007. Thermoregulation and aging. Am. J. Physiol. Regul. Integr. Comp. Physiol. 292, R99–R102.
Vande Velde, G., De Langhe, E., Poelmans, J., Bruyndonckx, P., d'Agostino, E., Verbeken, E., Bogaerts, R., Lories, R., Himmelreich, U., 2015. Longitudinal in vivo microcomputed tomography of mouse lungs: no evidence for radiotoxicity. Am. J. Physiol. Lung Cell Mol. Physiol. 309, L271–L279.
Vander Heiden, M.G., Cantley, L.C., Thompson, C.B., 2009. Understanding the Warburg effect: the metabolic requirements of cell proliferation. Science 324, 1029–1033.
Vinegoni, C., Aguirre, A.D., Lee, S., Weissleder, R., 2015. Imaging the beating heart in the mouse using intravital microscopy techniques. Nat. Protoc. 10, 1802–1819.
Vrachimis, A., Hermann, S., Máthé, D., Schober, O., Schäfers, M., 2012. Systematic evaluation of (99m)Tc-tetrofosmin versus (99m)Tc-sestamibi to study murine myocardial perfusion in small animal SPECT/CT. EJNMMI Res. 2, 2–21.
Waerzeggers, Y., Monfared, P., Viel, T., Winkeler, A., Jacobs, A.H., 2010. Mouse models in neurological disorders: applications of non-invasive imaging. Biochim. Biophys. Acta-Mol. Basis Dis. 1802, 819–839.
Wagenmakers, A.J., Strauss, J.A., Shepherd, S.O., Keske, M.A., Cocks, M., 2015. Increased muscle blood supply and transendothelial nutrient and insulin transport induced by food intake and exercise: effect of obesity and ageing. J. Physiol. 594, 2207–2222.
Wehner, J., Weissler, B., Dueppenbecker, P.M., Gebhardt, P., Goldschmidt, B., Schug, D., Kiessling, F., Schulz, V.V., 2015. MR-compatibility assessment of the first preclinical PET-MRI insert equipped with digital silicon photomultipliers. Phys. Med. Biol. 60, 2231.
Weissler, B., Gebhardt, P., Dueppenbecker, P.M., Wehner, J., Schug, D., Lerche, C.W., Goldschmidt, B., Salomon, A., Verel, I., Heijman, E., Perkuhn, M., Heberling, D., Botnar, R.M., Kiessling, F., Schulz, V., 2015. A digital preclinical PET/MRI insert and initial results. IEEE Trans. Med. Imaging 34, 2258–2270.
Wenning, C., Kloth, C., Kuhlmann, M.T., Jacobs, A.H., Schober, O., Hermann, S., Schafers, M.A., 2014. Serial F-18-FDG PET/CT distinguishes inflamed from

stable plaque phenotypes in shear-stress induced murine atherosclerosis. Atherosclerosis 234, 276–282.
Whitehead, J.C., Hildebrand, B.A., Sun, M., Rockwood, M.R., Rose, R.A., Rockwood, K., Howlett, S.E., 2014. A clinical frailty index in aging mice: comparisons with frailty index data in humans. J. Gerontol. A Biol. Sci. Med. Sci. 69, 621–632.
Wiesmann, F., Ruff, J., Hiller, K.H., Rommel, E., Haase, A., Neubauer, S., 2000. Developmental changes of cardiac function and mass assessed with MRI in neonatal, juvenile, and adult mice. Am. J. Physiol. Heart Circ. Physiol. 278, H652–H657.
Wiesmann, F., Frydrychowicz, A., Rautenberg, J., Illinger, R., Rommel, E., Haase, A., Neubauer, S., 2002. Analysis of right ventricular function in healthy mice and a murine model of heart failure by in vivo MRI. Am. J. Physiol. Heart Circ. Physiol. 283, H1065–H1071.
Willie, B.M., Birkhold, A.I., Razi, H., Thiele, T., Aido, M., Kruck, B., Schill, A., Checa, S., Main, R.P., Duda, G.N., 2013. Diminished response to in vivo mechanical loading in trabecular and not cortical bone in adulthood of female C57Bl/6 mice coincides with a reduction in deformation to load. Bone 55, 335–346.
Willmann, J.K., van Bruggen, N., Dinkelborg, L.M., Gambhir, S.S., 2008. Molecular imaging in drug development. Nat. Rev. Drug Discov. 7, 591–607.
Wolf, A.M., Nishimaki, K., Kamimura, N., Ohta, S.V., 2014. Real-time monitoring of oxidative stress in live mouse skin. J. Invest. Dermatol. 134, 1701–1709.
Wollenweber, T., Zach, C., Rischpler, C., Fischer, R., Nowak, S., Nekolla, S.G., Grobner, M., Ubleis, C., Assmann, G., Muller-Hocker, J., La Fougere, C., Boning, G., Cumming, P., Franz, W.M., Hacker, M., 2010. Myocardial perfusion imaging is feasible for infarct size quantification in mice using a clinical single-photon emission computed tomography system equipped with pinhole collimators. Mol. Imaging Biol. 12, 427–434.
Workman, P., Aboagye, E.O., Balkwill, F., Balmain, A., Bruder, G., Chaplin, D.J., Double, J.A., Everitt, J., Farningham, D.A., Glennie, M.J., Kelland, L.R., Robinson, V., Stratford, I.J., Tozer, G.M., Watson, S., Wedge, S.R., Eccles, S.A., 2010. Guidelines for the welfare and use of animals in cancer research. Br. J. Cancer 102, 1555–1577.
Wu, Y.L., Chu, D.T., Han, B., Liu, X., Zhang, L., Zhou, C., Liao, M., Mok, T., Jiang, H., Duffield, E., Fukuoka, M., 2012. Phase III, randomized, open-label, first-line study in Asia of gefitinib versus carboplatin/paclitaxel in clinically selected patients with advanced non-small-cell lung cancer: evaluation of patients recruited from mainland China. Asia Pac. J. Clin. Oncol. 8, 232–243.
Wunder, A., Tung, C.H., Muller-Ladner, U., Weissleder, R., Mahmood, U., 2004. In vivo imaging of protease activity in arthritis: a novel approach for monitoring treatment response. Arthritis Rheum. 50, 2459–2465.
Wyatt, S.K., Barck, K.H., Kates, L., Zavala-Solorio, J., Ross, J., Kolumam, G., Sonoda, J., Carano, R.A., 2015. Fully-automated, high-throughput micro-computed tomography analysis of body composition enables therapeutic efficacy monitoring in preclinical models. Int. J. Obes. (Lond.) 39, 1630–1637.
Yang, D., Xie, Z., Stephenson, D., Morton, D., Hicks, C.D., Brown, T.M., Sriram, R., O'Neill, S., Raunig, D., Bocan, T., 2011. Volumetric MRI and MRS provide sensitive measures of Alzheimer's disease neuropathology in inducible Tau transgenic mice (rTg4510). Neuroimage 54, 2652–2658.
Yang, H., Butz, K.D., Duffy, D., Niebur, G.L., Nauman, E.A., Main, R.P., 2014. Characterization of cancellous and cortical bone strain in the in vivo mouse tibial loading model using microCT-based finite element analysis. Bone 66, 131–139.
Yong, J., Rasooly, J., Dang, H., Lu, Y., Middleton, B., Zhang, Z., Hon, L., Namavari, M., Stout, D.B., Atkinson, M.A., et al., 2011. Multimodality imaging of β-cells in mouse models of type 1 and 2 diabetes. Diabetes 60, 1383–1392.
Zhang, X., Kuo, C., Moore, A., Ran, C., 2013. In vivo optical imaging of interscapular brown adipose tissue with (18)F-FDG via Cerenkov luminescence imaging. PLoS One 8, e62007.
Zhang, X., Tian, Y., Zhang, C., Tian, X., Ross, A.W., Moir, R.D., Sun, H., Tanzi, R.E., Moore, A., Ran, C., 2015. Near-infrared fluorescence molecular imaging of amyloid beta species and monitoring therapy in animal models of Alzheimer's disease. Proc. Natl. Acad. Sci. U. S. A. 112, 9734–9739.
Zhou, R.H., Vendrov, A.E., Tchivilev, I., Niu, X.L., Molnar, K.C., Rojas, M., Carter, J.D., Tong, H., Stouffer, G.A., Madamanchi, N.R., Runge, M.S., 2012. Mitochondrial oxidative stress in aortic stiffening with age: the role of smooth muscle cell function. Arterioscler. Thromb. Vasc. Biol. 32, 745–755.
Zlokovic, B.V., 2010. Neurodegeneration and the neurovascular unit. Nat. Med. 16, 1370–1371.